Preparation of bio-based powder for 3D printing applications by Selective Laser Sintering

Giorgio De Trane, s275514

December 3, 2022

POLITECNICO DI TORINO
Department of Mechanical and Aerospace Engineering

Master of Science in Aerospace Engineering

Supervisor: Prof. Massimo Messori
Co-supervisor: Prof. Giovanna Colucci

To my parents, whose love has always been unconditional, intense and at times hard to comprehend.

Abstract

The goal of this case study is to optimize the production of *Selective Laser Sintering* (SLS) suitable fine powders of sustainable bio-based polymers and directly assess their printability.

Among the bio-based polymers, PLA is the most widely used in the *Fused Deposition Modeling* (FDM) hobbyist and enthusiast markets, whereas more invasive polymers such as PA12 are commonly used in SLS, the most common 3D printing technology for the production of functional parts.

A higher demand for bio-based polymers in the SLS industry is expected in the near future - following the general sustainability goals of all industries - as the technology allows for the production of more complex geometries and intricate details, as well as ad-hoc parts for the medical industry, where the use of bio-based polymers is already widespread.

The catalogue of bio-based polymers available for SLS is currently expanding, but still limited, and the production of fine powders is a critical step in the process of producing functional parts.

This study focused on *polyhydroxybutyratehexanoate* (PHBH), a copolymer of the *polyhydroxyalcanoate* (PHA) family, with a wider sintering window and thus a higher potential for SLS applications, compared to other polymers of the same group.

An extensive research on current *state-of-the-art* production methods, most notably cryogenic mechanical milling and chemical precipitation, led to choosing the latter, since the former does not produce spherical particles, unless further heat treatments are applied, with unpredictable rates of success and potentially high power consumption.

An initial recipe for PHBH, previously tested by other researchers, has been tweaked and improved, achieving over a ten-fold increase in *pellet-to-powder* yield, compared to the very early stages of production.

PHBH microspheres were obtained by oil-in-water emulsion solvent evaporation method.

The process involves the dissolution of the polymer in chloroform, followed by dripping the viscous liquid in a water solution containing 0.25 $\%_{wt}$ of PVA and stirring the mixture, which leads to the complete solvent evaporation and the polymer precipitation as a fine powder.

The resulting powder is then cleaned, dried overnight and sieved, to obtain a final product with a particle size distribution suitable for SLS applications ($< 100\ \mu m$).

Specimens of the obtained powder have been collected and characterized by means of a series of tests, including various thermal analysis methods, such as TGA and DSC, as well as a flowability test and density measurements via a gas pycnometer.

The SLS suitability of the powder has been further assessed in terms of morphology by *Scanning Electron Microscopy* (SEM), which revealed a close to ideal distribution of predominantly spherical, non-hollow particles, as also confirmed by granulometry investigations.

The powder has been printed on an SLS 3D printer, with single layer and multilayer objects achieving a print quality comparable to that of standard SLS polymers such as PA12.

Complex geometries and intricate details have been successfully printed as a proof of concept, as well as prismatic samples.

Contents

List of Figures

List of Tables

1 Thesis Goal

The ever increasing demand for sustainable materials in all manufacturing industries has led to a growing interest in the production of bio-based polymers for various applications.
In particular, the interest for bio-based polymers in the *Additive Manufacturing* (AM) industry has skyrocketed in the last few years, along with the general interest in sustainable materials, and the use of bio-based polymers in 3D printing is expected to grow in the near future, with more research and resources being invested in the field, and costs decreasing as the market share increases.

Among the various AM techniques, *Selective Laser Sintering* (SLS) is increasing in popularity and maturing as a technology. This includes its applications with bio-based polymers themselves, which are already used in the medical industry, but are still limited in terms of the number of available polymers and the production of fine powders for SLS applications.

The current literature on the subject is still scarce and the available systematic reviews highlight the need for further research in the field, in order to expand the catalogue of bio-based polymers available for 3D printing and to optimize the production of fine powders for SLS specifically.

The goal of this thesis is to further explore the production of biopolymer fine powders for SLS applications, with a focus on PHBH and chemical precipitation, by optimizing the production pipeline, characterizing and directly assessing the printability of the resulting polymeric powder.

2 Introduction

AM is a broad term that encompasses several manufacturing techniques, characterized by their additive nature, as the name suggests, in contrast with more traditional subtractive processes.
AM techniques are applied to a wide range of materials, including ceramics, polymers and metal alloys, some of which are specifically developed or optimized for various kinds of applications, to the point that entire normatives have been introduced for their regulation [1].
The main advantage of AM is the ability to produce complex shapes in a relatively short time. These geometries are either too hard or even impossible to reproduce with subtractive manufacturing techniques, which often require multiple steps, using different pieces of equipment, trained personnel, etc [2].

Given the same material, the complex shapes allowed by AM can replace components made of multiple assembled parts with a unique solid piece of comparable or even better mechanical properties.
The inherent flexibility of AM often allows product designers to simplify or even entirely bypass the very strict CAD workflow (which is inherently tied to traditional manufacturing processes) and make use of organic and/or generative modeling, aided by advanced machine learning algorithms [3].
As a consequence of better design choices and minimal need of post-processing of AM objects, far less raw material is wasted, compared to subtractive manufacturing techniques, leading to long term lowering of costs, faster design-to-market pipelines and, last but not least, lower emissions and environmental impact [4, 5].

2.1 Polymers in Additive Manufacturing

Polymers and their composite materials have been used in all sorts of fields, ranging from arts and crafts all the way to advanced biomedical and aerospace applications, thanks to their unique and varied extended range of properties [4, 6–12].

The rapid advancement of AM, where polymers have been extensively used for prototyping, in the form of resins, filaments, powders and viscous inks, has increased the demand for high-performance polymers, in order to take advantage of their quicker printing times (compared to metals) as well as their lower cost, while still maintaining good mechanical properties for an end product, rather than just a prototype [4].

The urge for drastically reducing the environmental impact of human activities involves every production field, including AM, which can be inherently less impactful than traditional manufacturing processes, given the same material and final product to achieve.

A consequence of the concerns about climate change and its potentially catastrophic outcomes is the research in the field of eco-friendly materials, including polymers that could be used in AM.
An example is *polylactic acid* (PLA), a polymer widely used in 3D printing, whose monomer is obtained by fermenting starches, such as corn starch.

Many new eco-friendly polymers have been and are currently being studied for AM techniques, but this thesis focused mostly on materials that can be potentially turned into powders for *Powder Bed Fusion* (PBF) techniques or filaments for *Fused Filament Fabrication* (FFF).

2.2 Common AM techniques for polymers

Polymers can be processed with several AM techniques, including, but not limited to:

- **VP** (*Vat Photopolymerization*), which makes use of UV light (or other radiations) to solidify photosensitive resins. This class of AM processes can produce parts with the highest resolution among all AM methods [4, 11];
- **MJ** (*Material Jetting*), which consists of a deposition of viscous fluids (either in droplets or in a continuous fashion), solidified by different agents (time interacting chemicals, heating, cooling, drying, photopolymerization, etc.). These processes include several patented methods, characterized by high speed printing [4];
- **PBF** (*Powder Bed Fusion*), where the object is printed by locally fusing a powder bed (with a pulsing energy source -such as lasers- or with a local deposition of chemicals), layed out in a layer-by-layer fashion [4, 11];
- **ME** (*Material Extrusion*), where each layer is printed by direct deposition of materials through a nozzle, that solidify as they cool down [4, 11];
- **BJ** (*Binder Jetting*), similarly to 2D inkjet printing utilizes a polymer in the form of a liquid binder, that gets deposited in droplets onto a powder bed (usually made of metallic or ceramic particles). This method can build large parts without support structures and the lack of a high power heat source cuts its cost down, but the structural properties of the final parts are poor compared to sintered equivalents, making heat treatments necessary [4];
- **Sheet Lamination**, where thin sheets of material are stacked together and bonded with adhesives or heat. This class of techniques is not entirely additive, since subtractive processes are used to cut and refine the final part, creating substantial material waste [4].

2.2.1 Selective Laser Sintering (SLS)

SLS is a manufacturing process in the PBF family.
A powder bed is layed out onto a platform and a focused heat source (a laser) locally sinters the powder, until a single layer is completed [4, 11].
A mechanism wipes out the remaining powder, which is recollected and automatically redistributed by a recoating system, for each subsequent layer [13].
This process is similar to *Selective Laser Melting* (SLM), typically used with metal alloys: in SLS the energy input is not high enough to bring the powders to their melting point, but sufficient for sintering of the powders.
Despite the slight difference, many sources use both terms interchangeably, often effectively referring to SLM in metal manufacturing.
When it comes to thermoplastic materials, the required laser power to sinter each layer is substantially lower than that needed for metals.

SLS printers can be considerably more expensive than *Fused Deposition Modeling* (FDM [1]) machines of similar printing volume, but the advantages they offer, in terms of customizability, superior consistency in print quality and accuracy, higher production rate, less need for support structures, makes them a more cost effective solution for larger scale industrial production, whereas FDM printers are still more established in the hobbyists and enthusiasts market [13].

Generally speaking, SLS is a three stage process [13], consisting of:

- warming up (A)
- building (B)
- cooling (C)

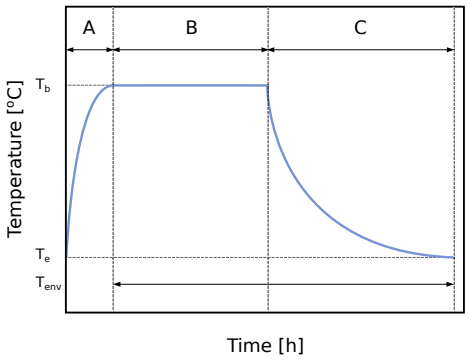

Figure 1: Phases of an SLS process, adapted from [13]

[1] FDM is a more common name for the FFF technique explained in section 2.2 and is often generically named 3D printing in mass media.

As seen in Figure 1, the first phase is the time required to reach a specific powder bed temperature (T_b), based on the material of choice.
Ideally this temperature should be maintained constant inside the printing chamber, during the entire building phase, through infrared or electric heaters. The main goal is avoiding drastic temperature gradients in different areas of the printed part, since they can cause visual artefacts such as local or global deformation and, most importantly, uneven residual mechanical tension that can rapidly degrade the structural integrity of the final piece, especially in structural components that might be placed under static or dynamic loads.

Once the final piece is printed, the entire chamber is cooled down homogeneously and gradually, until the equilibrium is reached at room temperature (T_e) [13].

Quality standards for SLS printed parts have increased dramatically over the last few years, to the point where the manufactured components are not exclusively used for prototyping or as sacrificial items for investment casting, but they are used as finalized industrial grade parts.
However, there is still room for substantial improvements in the consistency of print accuracy, overall quality, reliability and scalability of the entire process, compared to more traditional manufacturing techniques.

The variety of interdepent physical phenomena involved in SLS and their different temporal regimes are the main sources of complexity that makes the process inconsistent and very hard to study.
The most predominant phenomena are the following [13]:

- Laser motion and irradiation
- Thermal diffusion
- Polymer viscous flow and particles coalescence
- Powder spreading
- Solidification/crystallization

Further improvements are required in order to reduce the amount of discarded parts (still comparatively higher than most consolidated manufacturing techniques), usually defective in terms of porosity or thermal distortion or warping [13].

3 Polyhydroxyalkanoates (PHA)

Bio-based polymers are a promising alternative to traditional petroleum-based materials, due to their lower environmental impact and their potential to be produced locally, in a sustainable way [8, 11, 14, 15].

These materials are typically produced by microorganisms, through a process called *bioplasticization*, which is a form of *biomass conversion* [11].
This process is based on the ability of some microorganisms to convert a wide variety of carbon sources, such as sugars, starches, cellulose, fats and oils, into ready to use polymers or precursors, tipically in anaeroobic conditions.
The most common microorganisms used for this purpose are bacteria, which are able to produce a wide variety of biopolymers, including *polyhydroxyalcanoates* (PHA) [11].
PHAs are a family of bio-based thermoplastic polyesters, obtained by hydroxyalkanoic acids via bacterial fermentation, under nutrient depletion and carbon excess conditions [8, 11].
They are a sustainable alternative to petrochemical polymers commonly utilized in additive manufacturing and they are mostly used for prototyping in the medical field [8, 11].
Similarly to other sustainable plastics, PHAs can be produced using industrial byproducts as substrates (corn, soy, coffee, oil wastes, etc.) [11].

The monomer composition of PHA can be very diverse, depending on the microorganisms involved and the fermentation medium.
This variety impacts the overall mechanical, thermal and chemical properties of the final plastic, which depend on the concentration of different monomers in polymers and copolymers.
PHAs can be classified by the chain-length of their monomers [8]:

- *scl-PHA* (short-chain-length PHA) with 3 to 5 carbon atoms
- *mcl-PHA* (medium-chain-length PHA) with 6 to 14 carbon atoms
- *lcl-PHA* (long-chain-length PHA) with more than 14 carbon atoms

Estimating the exact meaningful measures of their properties is not always a straight-forward process, since manufacturers are not transparent about the exact composition of their products, which may have been improved by proprietary additives, whose concentration and exact composition are not usually fully disclosed [11].

The market for bioderived PHA has gradually increased over the years and the growth is estimated to keep its pace, considering that not only are they more sustainable than competing petrochemical polymers, but they offer additional valuable properties, such as piezolectricity and protection against gases and UV light [11, 16].

Their bio-origin, non-toxicity, renewability, biodegradability and biocompatibility make PHAs a very compelling product in the ever growing market of sustainable materials.
However, these desirable qualities contribute to their higher price, which is still not competetive against more established polymers of similar properties [11, 17]. The increasing demand and the improvements on their biosynthesis are expected to make the price more accessible in the future, for all sorts of applications, including AM, where PHAs can be printed successfully either with FDM or SLS techniques [11].

3.1 PHA and Additive Manufacturing

PHAs can be used in different AM techniques, including *Stereolitography*, which is part of VP processes, FFF, where the filaments are often made of a PHA-PLA blend, (which increases thermal stability and cuts down cost), and SLS [11].

This thesis work focused on its usage in SLS.

PHAs have been successfully printed via SLS and utilized in the medical field as scaffolds for tissues engineering applications [8].
These scaffolds can be printed with a porous structure (controlled by the laser energy density), which could aid in carrying biomolecules and slowly release drugs, for instance [8, 15].
Unlike with FDM applications, where PHA can not be used as a standalone filament, but needs PLA addition in order to stabilize its melting phase, PHA powders for SLS tend to maintain a better stability and their chemical composition does not get altered as easily.
This is a clear advantage, since general properties of the final products do not change drastically from its starting feedstock, and, in addition to this, the remaining powder is not thermally altered in proximity to the melt pool, meaning that it can be reused for additional printing [11].

3.1.1 Poly(3-hydroxybutirate-*co*-3-hydroxyhexanoate) (PHBH)

PHBH is a copolymer of the PHA family (molecular structure in Figure 2), which gained interest in the AM field and specifically in SLS applications, since it has a wider sintering window than other polyhydroxyalkanoates such as PHB and PHBV [2, 9].

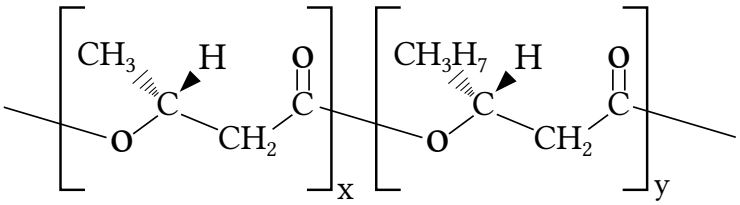

Figure 2: Schematic representation of the PHBH polymer structure.

Despite having gained attention in the PHA family for SLS, especially in academic environments, the general interest for this copolymer is still relatively lower than other petrochemical polymers, due to its early-stage synthesis process, its cost and the strict confidentiality of polymer manufacturers [18].

4 Powder production for SLS

Manufacturing raw materials for FDM is a relatively easy process, since the plastics need to be mass produced into filaments or pellets.
However, producing powders from plastics is a much more convoluted process [4, 9, 19].

Two radically different approaches are possible, each with its own critical issues:

- Mechanical milling
- Chemical precipitation

4.1 Powder requirements for SLS

The success rate of SLS prints is highly dependent on the characteristics of the powders involved.
The key factors in powder quality are particle size distribution, morphology, as well as thermal, flow and optical properties.

Ideally, a gaussian distribution, with most particles close to the average size is desirable, with a tipical range of $(20 \div 80)\ \mu m$ [9].
The average particle size directly influences the layer thickness in the SLS process.
Powder morphology is crucial in the sintering mechanism, where regular, smooth and non-hollow spherical particles are preferable in order to effectively obtain sintering necks, as illustrated by Figure 3 [9].

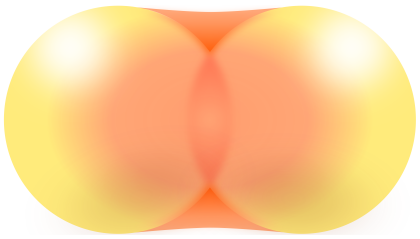

Figure 3: Two spherical powder particles forming a sintering neck

The powder's density is another parameter that should be considered, as it directly correlates with the final part's global density and it allows calculation of the Hausner ratio H_r (as seen in equation 1), which is a direct predictor of powder flowability.
Ideally, this coefficient should be lower than 1.4, otherwise the powder could result in issues with fluidization [9].

$$H_r = \frac{\rho_{tap}}{\rho_{bulk}} \tag{1}$$

where ρ_{tap} is the tap density and ρ_{bulk} is the bulk density of the powder.

Understanding thermal properties of the powder is essential in SLS.
SLS is characterized by an optimal sintering window, with a temperature range between crystallization (T_c) and melting (T_m). For any given heat flow within that range, the material is in a metastable phase, where full coalescence of the top powder layer, as well as adhesion with previously sintered layers are most likely guaranteed [9].
Therefore, creating a tailor-made powder feedstock involves using materials with a wide enough sintering window [2, 9].

Furthermore, optical properties of the powder bed need to be taken into account, since highly reflective materials (for a given laser wavelength) can waste most of the energy input, instead of absorbing a significant amount of radiation needed to effectively melt the powder [9].
This issue is prevalent in metal SLM, as previously mentioned [6, 9].
When it comes to SLS and plastics powders, a significant advantage is that the required energy is substantially lower than that needed to melt metal alloys, meaning that any potential problem with poor radiation absorbtion can be compensated by increasing the laser power output with relative ease [9].

Viscosity and surface tension of the melt pool are more relevant factors when choosing powders for SLS. High viscosity and surface tension can hinder the coalescence of polymer powders and the adhesion with previously sintered layers, resulting in residual sheer stress, high porosity and thus poor quality of the 3D printed part in general [13].
In SLS, unlike other processes i.e. investment casting or injection molding, there is no well distributed force (e.g. built up pressure against the mold) that can increase particle coalescence and layer adhesion. The only relevant force acting on the printed part is gravity, along the vertical axis [9].

4.2 Mechanical milling

Grinding plastics into fine and homogeneous powders can be a challenge, since the high speed milling devices can easily overheat the plastics above their softening point, creating lumps of material, far from the desired result.
A solution to this problem is using so called *cryogenic grinding* devices, which utilize cooling agents such as dry ice, liquid carbon dioxide or liquid nitrogen, in order to keep the plastics below the glass transition point, where polymers become intrinsically brittle, similarly to a ceramic material, making it possible to turn the original mass into a powder [20].
The heterogeneous powders can later be sieved and separated, based on their different granulometry.

Despite being an effective process for powder production, the morphology obtained with cryogenic milling is extremely irregular and unpredictable, which makes this method generally unsuitable for high quality SLS parts [9].

4.3 Chemical precipitation

There is little variety in the market of SLS ready polymer powders, with *polyamide-12* (PA12) being the most optimized for this application and being produced by precipitation in ethanol [2].
Many other polymer powders can be produced using the precipitation method, but their development is currently very limited and in early-stage, especially with thermoplastics, which are not as optimized as PA12 [11].
Most of the experimental work on the precipitation method for thermoplastics is not made available by large chemical corporations, but rather by academic environment [11].

4.3.1 Polymer-Solvent System

Assuming there is a potential material to use this technique with, the recommended solvent choice gravitates towards so called *moderate solvents* [2].

These compounds have the peculiarity of acting as a solvent only when heated above a certain temperature.
Therefore, thermoplastics can be dissolved into a compatible solvent and form a liquid-liquid phase separation upon cooling of the system, where complex crystallization and precipitation phenomena are later induced via stirring of the nucleated polymer-rich droplets [2].

A common criterion of solvent pre-selection is the evaluation of Hansen parameters, through the following equation 2:

$$f(\delta_x) = 100 \cdot \frac{\delta_x}{\delta_d + \delta_p + \delta_h} \tag{2}$$

which quantifies the interaction between the polymer and the solvent, in correlation with the dispersion (δ_d), the polar interactions (δ_p) and the hydrogen bond interactions (δ_h) [2].
Once the polymer-solvent system is tested, the experimental data can be effectively represented in the TEAS plot (as shown in Figure 4), which helps visualizing equation 2.

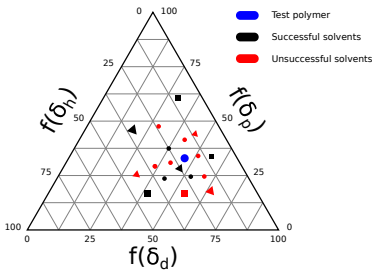

Figure 4: Generic TEAS plot for any given polymer [2]

This approach has been successfully used to determine solubility of *polypropylene* (PP), *polyethylene terephthalate* (PET), *polycarbonate* (PC), etc, and could be effectively utilized with bio-based polymers such as PHBH [2].

4.3.2 Cloud point diagram

After choosing a suitable moderate solvent, the process needs to be studied and quantified with a cloud point diagram of temperature, as a function of polymer weight concentration, allowing the identification of a dissolution temperature and the temperature where *liquid-liquid phase separation* (LLPS) occurs [2, 21]. These measures allow better scalability of the process in larger controlled environments such as a reactor or autoclave system [2].

4.3.3 Production in a controlled environment

The cloud point diagram data allows for an optimization of the production process in autoclave or reactor system.
Temperature profile, initial polymer concentration and, most importantly, stirring conditions can greatly influence the final particle size distribution.
Stirring is the most impactful of these factors, producing smaller particles as the intensity increases [2], as reported in Figure 5.

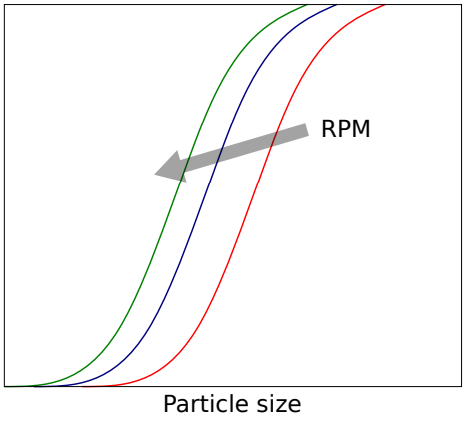

Figure 5: Particle size decreases as stirring RPM increase

4.4 Environmental impact

At first glance, cryogenic milling seems to be a more sustainable option for powder production. However, the aforementioned issues make this method unsuitable for SLS, unless future developments will consistently improve overall powder morphology, perhaps with the aid of post processing via thermal rounding of the particles [2].

On the other hand, while powder production by chemical precipitation produces much better and more controllable powder feedstock, it is worth noting that organic solvents are intrinsically environmentally impactful and that should be taken into account, especially for large scale production of these powders.
The entire purpose of utilizing sustainable bio-based polymers in the first place might be rendered pointless, if their powder production utilizes compounds or processes that are not environmentally friendly [22].

Better innovative solutions (or mitigations of the mentioned issues in the current pipelines) need to be implemented in the near future.

Thermal rounding is a heat treatment, aimed at improving the bulk powder morphology for SLS applications. This kind of treatment might be the crucial step in the success of a more environmentally friendly pipeline, which does not involve any polluting solvent.
Powders can be heated either directly, with a carrier gas, or indirectly, using heated walls.
While the former method has a better process yield and reduced risk of lumping, the latter produces powders with a better, more spherical morphology, but with a significantly higher risk of particle agglomeration [19].

5 Choice of material and production process

As seen in previous chapters, this thesis work focused on PHBH, mainly for its wider sintering window, among all PHAs.

An early stage precipitation reaction had already been developed for PHBH, by other teams involved in the research [8]. This initial recipe has been tested out with the other bio-based polymers as well, but PHBH held the most promising results even in its early stages.

Other approaches such as cryogenic milling have been taken into consideration, but quickly discarded, due to the lack of equipment suitable for thermal rounding treatments.
The grinding procedure, aided by liquid nitrogen, proved to be successful at producing fine powders, according to the literature [19].
However, unless a thermal rounding treatment is applied, the powder morphology is too irregular and far from the ideal spherical geometry, thus making the obtained batches unsuitable for 3D printing [19].

All of the mentioned points led to definitely choosing PHBH for this thesis work, focusing on the optimization of the available blueprint for a suitable chemical precipitation process, as explained in the following chapters.

6 Initial chemical precipitation recipe for PHBH

As mentioned earlier, a prototype for a chemical precipitation reaction had already been developed, derived from experiments on solute-solvent compatibility (see Figure 4), which highlighted a good affinity between PHBH and chloroform.

Starting from a 4 g batch of PHBH pellets, the highest amount of sieved powder ($< 100\ \mu m$) ever produced was around 1.2 g, resulting in a 30 % maximum yield.

The very early experiments were conducted using a trial and error approach, with the issues previously discussed playing a major role in the reaction's rate of success.
After thoroughly studying the process in all its phases and isolating different parameters that could have caused the issues, the recipe has been tweaked by addressing the key variables, as later discussed.

6.1 Materials

The ingredients and quantities of the prototype reaction were the following:

- 4 g of PHBH pellets
- 55 ml of chloroform
- 400 ml of 0.25 $\%_{wt}$ of PVA solution

Despite its apparent simplicity, the reaction is highly influenced by the environmental conditions, as well as equipment's correct use and proper operability.

Any slight deviation from the correct parameters, whether due to unpredictable changes in environmental conditions, malfunctioning or incorrect use of the available tools, could in fact potentially break the unstable equilibrium of the reaction, making it extremely hard to pinpoint the exact root cause of failure.

Several failed attempts, changes in equipment and tools, as well as quantities were required in order to understand the most relevant parameters of the entire process.

6.2 Detailed step-by-step reaction

The reaction is shortly described by the following diagram:

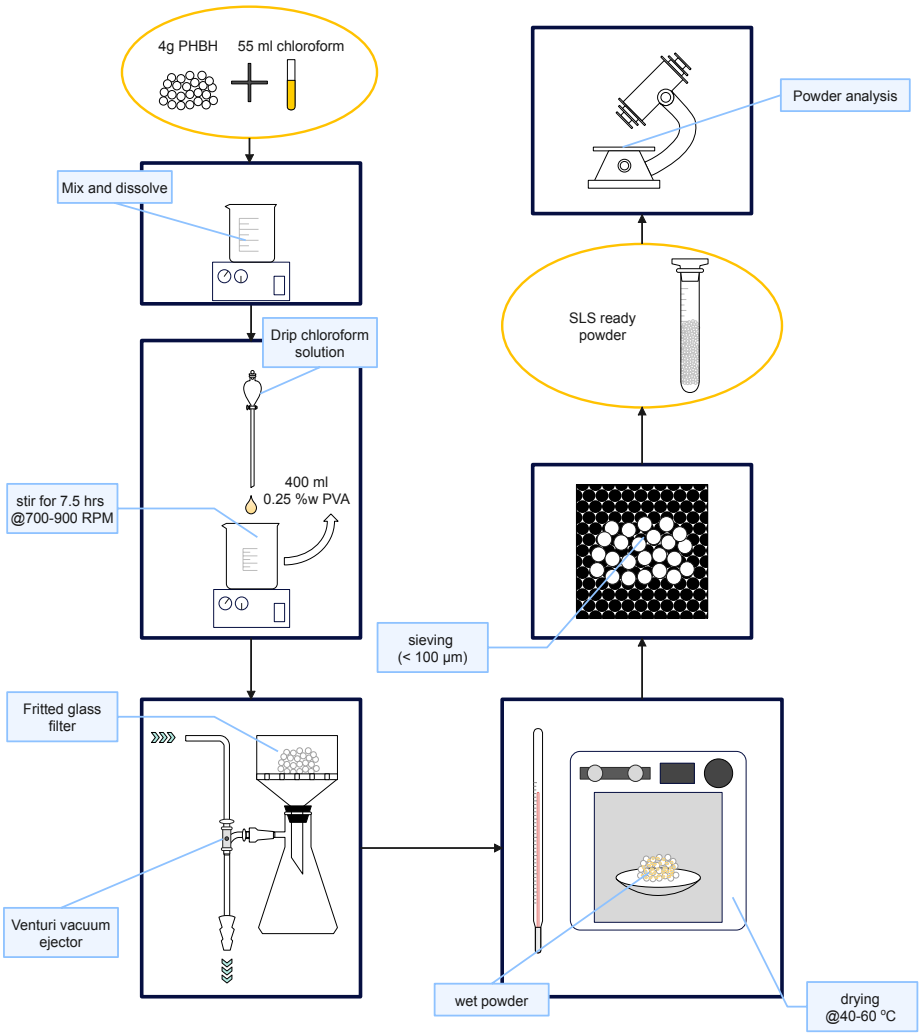

Figure 6: Process diagram describing the entire powder production pipeline

PHBH pellets (4 g) were dissolved into 55 ml of chloroform, in order to create a viscous liquid that has later been slowly dripped into a 0.25 % PVA solution, where the precipitation phenomenon occurred for a duration of 7.5 hours, at 700-900 RPM.

It is important to highlight that way too low stirring speeds resulted in a long mixing time and excessive evaporation of chloroform, which lead to higher viscosity and issues with the formation of fine powders during precipitation, as previously discussed.

On the other hand, splashes and foaming occurred at excessively high stirring speeds, causing loss of liquid, or hindering the visual inspection of the solution. A visual inspection of the solution is essential, as the presence of undissolved PHBH granules or impurities can obstruct the dripper or potentially drastically reduce the final yield.
Chloroform tended to dissolve the pellets' surface extremely quickly, creating a film around each granule, that could potentially stick them together or to the container, which lead to a significant delay in total dissolution time.
As best practice, this issue has been addressed by slowly dropping PHBH pellets into cloroform while already being stirred, instead of pouring the solvent onto the granules.

Dilution to the required fraction of mass was simply obtained by using 100 ml of 1 % solution, plus 300 ml of water, for a total of 400 ml.

The precipitation reaction was left stirring for 7.5 hours under a chemical hood, starting from the very first drop of PHBH-chloroform solution.
This time frame was extremely conservative, as it is very likely that all the residual chloroform evaporated in a much shorter time, however this aspect has not been tested yet.

At the end of the waiting time, the solution was washed and then filtered with a fritted glass filter, aided by a vacuum ejector.
The obtained powder bed was oven dried at 40 $^{\circ}C$, overnight.

At this point, the powder was completely dry and ready to be sieved.

A 100 μm sieve has been utilized, however, smaller size sieves could potentially be used, as many reviews recommend a particle size of $20 \div 80$ μm for SLS [13].
Sieved powders have been immediately stored in test tubes or any other sealable container, as PHBH is extremely hygroscopic.
With very fine powders, electrostatic interactions with tools and materials have been taken into account, when transferring them into containers.
However, choosing appropriate tools and avoiding unnecessary material transferring operations has been essential to minimize powder loss.

7 Recipe tweaking and improvements

All of the aforementioned attempts led to an optimization process that originally aimed at matching the 30 % yield obtained by previous researchers, but later far exceeded the initial expectations, improving upon the available blueprint procedure by a wide margin.

7.1 Key variables

Dealing with a simple yet unstable process, based on theoretical studies and very rough experimental data, requires a long trial and error approach, that should carefully isolate each variable, whether it is intrinsic to the involved physical and chemical reactions, environmental, equipment related, or introduced by human interaction with the process.

Generally speaking, once all the independent variables are isolated and understood, only a few are extremely relevant and can radically influence the success rate of the entire process.
Should these variables be changed, even unintentionally and by a small amount, the final yield could be dramatically cut down.

It has been pointed out several times that the reaction temperature is one of the most influential parameters of the entire process, given the fast evaporation pace of chloroform.

For all the issues discussed in previous chapters, an increase in temperature correlates with an increase in chloroform use.
The average maximum amount of chloroform (per 4 g of PHBH pellets) was estimated to be around 55 ml.
Attempting to use extra chloroform and higher temperatures stalled the results, and it proved to be detrimental over a certain threshold ($>$ 75 ml), as insufficient viscosity would prevent an accurate flow control during the dripping phase.

Adjustments in chloroform amounts were directly correlated with operational temperatures and the proper quantity should be used accordingly. A 10 ml increase in chloroform use might seem insignificant at a lab scale, but this translates to significant waste, assuming the process could be scaled to an industrial level and that no solvent retrieval system is available.
Overall, the key parameter that is controlled by temperature and that actually matters the most is viscosity: very low temperatures can minimize chloroform evaporation, but directly increase density and thus viscosity; on the other hand, liquids at higher temperatures should be inherently less viscous, but the drastic solvent evaporation dramatically increases viscosity, simply by having more PHBH and less liquid proportionally.

The process should be tailored to obtain a PHBH-chlofororm solution with the ideal viscosity, that allows a perfect dripping phase, while producing the highest pellet-to-powder yield.
By contrast, other variables like dripping flow (a drop by drop fashion is ideal but occasional flow distruptions do not seem to have a great influence), or a very precise measure in PVA concentration have not been deemed as important for the success of the precipitation process.
Assuming the adjustment of viscosity and the optimization of the dripping phase have been dealt with, another relevant parameter is the stirring speed of the PVA solution (see Figure 6 for reference).
The experiments conducted during this thesis confirmed what had already been found in the scientific literature: an increase in stirring speed directly correlates to a decrease in average powder particle size, as reminded by Figure 5 [2].
This correlation is generally measured in terms of RPM, which is an active control of any magnetic stirrer and a good indication of the average rotational speed of the stirred fluid, assuming that the device is properly functioning and every other variable is fixed.
This aspect is later discussed in further detail in section 7.2.

Increasing the stirring speed has proven to be an effective strategy to increase final yield: values in the range of $700 \div 900$ RPM consistently produced almost no waste during the sieving phase.

7.2 Adaptations and progressively refined equipment choice

Some of the initially chosen equipment was not perfectly suited for the necessary tasks and better choices have been made, as the understanding of the process has been refined.

For instance, the drippers used for the precipitation reaction had a manual flow valve, which made flow control unpredictable and hard to regulate.

Different magnetic stirrers have been utilized, however, a discrepancy in stirring speeds was noticeable, and the issue was addressed by uniforming the pipeline with identical models from the same manufacturer, which used the exact same settings.
Transferring and storing fine powders required some extra care as well. With average particle sizes under $100\ \mu m$, electrostatic interaction and powder volatility proved to be challenging when handling the final product.
Sieved powders have been transferred to test tubes or other comparable containers by using folded parchment paper.

All the workarounds and adaptations can normally be part of a very experimental lab workflow, but the process should ideally be capable of producing even greater yields, once it is scaled for industrial production, where each step is standardized and custom equipment tailored to specific tasks.

7.3 Current results in the powder production pipeline

Compared to the earliest batches, even the experiments conducted by previous researchers held substantially better results, with maximum yields of 30 %.

The minimum requirement for the current thesis work was that of replicating the previous records but, after a huge amount of failed attempts, optimization and tweaking in the entire process pipeline, current results far exceed the initial expectations, with even more room for improvement in the future.

The pellet-to-powder yield has increased to a minimum of 5 g of powder and a maximum of 6 g, over 8 g of raw material.
The current yield ranges between 62.5 % and 75 %, which is a relative improvement of $2 \div 2.5$ times that achieved in the previous research that this work is based on, and over an order of magnitude increase compared to the initial experiments.

Most noticeably, the process is very experimental for an SLS novel material such as PHBH and yet the results are a very remarkable achievement, considering the initial lack of a clear understanding of the precipitation process and the far from exhaustive literature on the specific subject.

At the current time of writing this thesis, no other known research work has been able to showcase a similar yield for the production of PHBH powder.

7.3.1 Consistent reproducibility and scalability

Not only has the total yield been improved, but the process has been stabilized and better understood in all of its peculiarities.
Until all the optimization work had been accomplished, the process held inconsistent results, with powder quantities drastically varying from insignificant to mediocre yields.

A key aspect of a reliable process is in fact its consistent reproducibility under known and controllable conditions, which is necessary (but not sufficient) for large scale production and adoption at industrial scale.

As previously mentioned, the latest results have been remarkable in terms of yield, but also in terms of consistency and reproducibility in the lab, which leads to believe even greater results could be achieved, when scaling the pipeline to industrial production standards.

8 Powder granulometry and morphology

While obtaining some form of powder with the precipitation process was somewhat expected, all the work would be pointless if the criteria discussed at the beginning of this research were not met.

The powders produced would not be suitable for SLS additive manufacturing, if granulometry (average grain size distribution) were not under a certain size threshold and if the morphology of those powders were not close to a non hollow spherical geometry [13].

While an adequate maximum size threshold is guaranteed by sieving the powders, investigations in terms of particle size distribution are needed in order to evaluate the overall granulometry.
In addition to this, adequate morphology can only be determined by visual inspection of *Scanning Electron Microscopy* (SEM) images, as explained later.

Sieving is an essential step when selecting SLS suitable powders.
A general guideline on SLS powders granulometry is that particles should be smaller than 100 μm, with many sources in the literature reporting an ideal range of $20 \div 80$ μm [13].

The powders obtained during the very first experiments produced a lot of waste during the sieving phase, which was due to their excessive size.
However, with the currently optimized process, the powder batches produced little to no waste during sieving, which has been achieved with a 100 μm sieve.

9 Powder and 3D printed parts characterization

The powder produced by the precipitation process has been characterized in terms of granulometry, morphology, gas pycnometry and flowability, as well as thermal properties, as later discussed in detail in chapters .

As all the mentioned analyses highlighted excellent results, well within the desired SLS requirements seen in section 4.1, the powder has been successfully used to produce 3D printed parts, which have been characterized in terms of mechanical properties, as well as thermal properties, that have been compared to those of the powder and the original raw material.

Overall, all of the analyses have shown that the PHBH powder produced by the precipitation process is suitable for SLS additive manufacturing, which is in itself a huge achievement for a novel and experimental process, given the fact that the powder is produced from a bio-based polymer that is not commonly used in the additive manufacturing industry, and that the available literature on the subject has highlighted the difficulty of obtaining SLS suitable powders from biopolymers [13].

Moreover, in addition to producing an SLS suitable powder, with an excellent yield, the 3D printing process has been successful as well, with a lot more potential to be explored in the future.

As a final note, one of the main goal of the carried out analyses was to address the potential change in thermal properties of the biopolymer, during the entire pipeline.
As shown in detail in the following chapters, both the powder and the printed parts have shown no significant thermal properties changes, compared to the original raw material, which is an extremely important aspect, given how bio-based materials are tipycally more sensitive to thermal degradation.

9.1 Scanning Electron Microscopy (SEM) analysis

Scanning Electron Microscopes are widely used detection instruments, which unlike traditional microscopes do not utilize optical lenses, but reconstruct images generated by the interaction between an electron beam and the targeted sample.

There are several inspection techniques that could be exploited using different SEMs, however the most suitable for inspecting fine powder morphology is the image reconstruction through *Secondary Electrons* (SE) emission.
When invested by a high energy electron beam, the inelastic interaction with secondary low energy electrons ($< 50\ eV$) triggers their emission from the valence bands of the specimen atoms and scatters them.
The emission of secondary electrons happens within a few nm inside the specimen, which makes this method perfectly suited for highlighting particle overall shape and surface displacement, to a high degree of detail and precision.

SEM images have been produced with multiple specimens, on samples collected during the entire duration of the experimental activities, which is later discussed in detail.
The expected particle morphology should ideally approach that of perfect non hollow sphere, as pictured in Figure 7, generated by *Dall-E 2*'s prompt-to-image artificial intelligence algorithm.

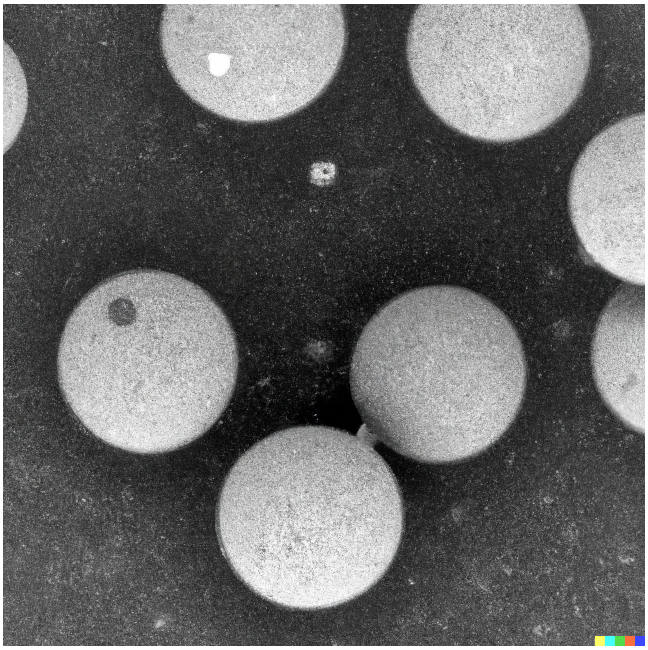

Figure 7: Prompt: *"Round particles seen through a SEM microscope"*

As mentioned, samples have been collected throughout the entirety of the experimental activity, which has been characterized by a lot of trial and error, before the entire production pipeline got optimized and under perfect control.

The experiment has been conducted using a *FIB-SEM, TESCAN S9000G, Tescan* instrument, which is a high resolution scanning electron microscope, equipped with a focused ion beam (FIB) for sample preparation and an electron backscatter diffraction (EBSD) detector.

The collected specimens have been selected, categorized and then assigned an ID:

$$ID = SEM_{NN} \tag{3}$$

where NN is the sample's absolute ascending time number.

The samples have been collected in a total of 12 different occasions, with a total of 12 different specimens.

The main instrument parameters to be modified during the experiment were the electron beam energy, the working distance, the magnification factor and the signal type.
The electron beam energy has been set to 10 kV for the first 6 samples, using the secondary electrons signal at constant pressure (SE) and then to 20 kV for the remaining 6 samples, using the variable pressure secondary electrons signal (VPSE G4).

Different magnification factors have been used, ranging from 400 to 800 X, to showcase different particle sizes and to better understand the particle morphology.

All SEM images have been AI upscaled and enhanced with basic raster image editing workflows, as shown in Figure 8.

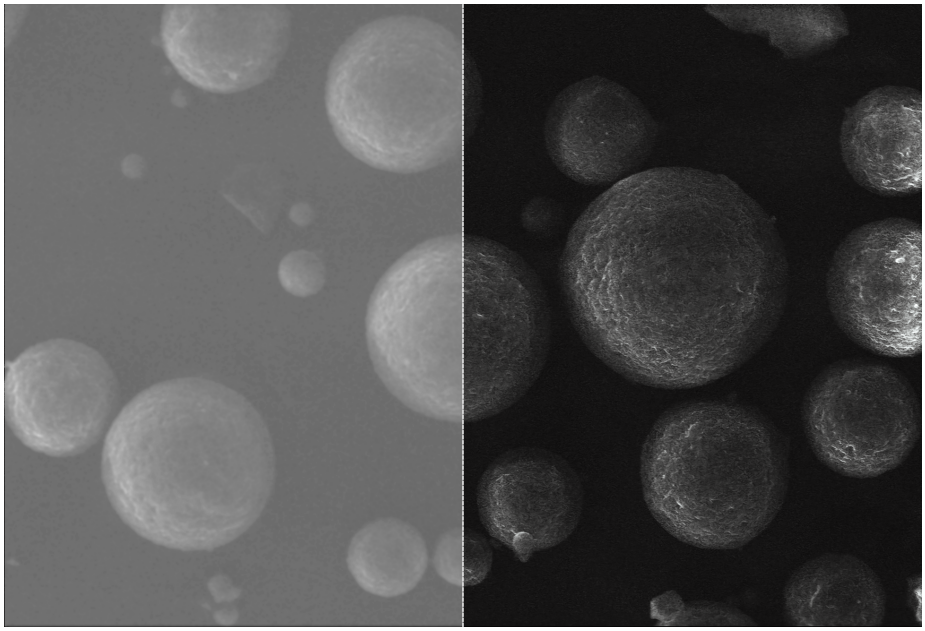

Figure 8: Example of a SEM image before and after enhancing

The most relevant pictures are showcased in chapter 11.1.

9.2 Thermal analysis

Various thermal analysis tools have been utilized in this thesis work, as many critical properties of the studied material can be deducted with different measurments at various temperature ranges.
This is especially true with materials suited for SLS, where knowledge of thermal properties is essential in determining a polymer's feasibility for this AM method. The thermal analysis tools used in this case study are the *Differential Scanning Calorimetry* (DSC) and the *Thermogravimetric Analysis* (TGA).

9.2.1 Differential Scanning Calorimetry (DSC)

DSC is a thermoanalytical technique that can be implemented with different types of machines, but its general purpose is the analysis of the change in heat flow as a function of temperature, which is generally increased in a linear fashion. The term differential in DSC indicates that each test sample is analyzed in parallel to a reference sample, whose heat capacity and thermal properties are well known and used to calibrate the machine.

A typical use of DSC is the detection of phase transitions, which is crucial for applications such as SLS, where each material needs to be locally fused within an optimal sintering window [10, 13].
One of the greatest advantage of PHBH over comparable materials is its wider sintering window, which makes it ideal for SLS [11, 18].

This sintering window can be measured by analyzing a DSC plot of heat flow over temperature, given that this test measures phase transitions (including crystallyzation) but is also capable of detecting more subtle physical changes, such as glass transition.
Since the sintering window is defined as the temperature range comprised between cold crystallization offset and melting point onset, then calculating it is trivial, based on the available results, which are highlighted in section 11.3.

The DSC machine used in this thesis work is the *DSC 214 Polyma Equipment* by Netzsch Group, which is a benchtop instrument that can be used for a wide range of applications, shown in Figure 9.

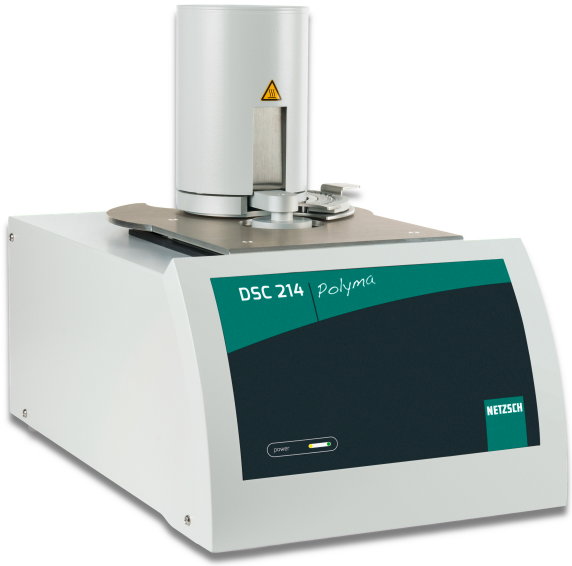

Figure 9: DSC 214 Polyma Equipment by Netzsch Group

It is equipped with a gas controller and has been used in the temperature range from $-50\ ^{\circ}C$ to $180\ ^{\circ}C$ with a heating rate of $10\ ^{\circ}C/min$, and from 180 to $-50\ ^{\circ}C$ with a cooling rate of $10\ ^{\circ}C/min$, under nitrogen flow ($50\ mL/min$).

The included software allows for the analysis of the DSC data, as well as the creation of a report with the results.
Multiple DSC analysis have been conducted and specimens have been catalogued with the following ID:

$$ID = xDSC_{NN} \tag{4}$$

where x is either g for granule or p for powder, and NN is the sample's absolute ascending time number.

9.2.2 Thermal Gravimetric Analysis (TGA)

TGA is a technique that constantly measures the mass of an object subjected to a deliberate change in temperature for a certain period of time, through a precision scale.
Time, temperature and mass are the involved variables and while mass is a direct measure, whose sudden changes (visible peaks in the weight vs temperature plot) can indicate relevant transition points, time and temperature are directly controlled as machine parameters.

Generally speaking, TGA instruments can be set up for different workflows:

- static or isothermal analysis, where weight changes are registered over a specified time frame, at a fixed temperature of interest
- quasi-static analysis, where temperature is changed in discrete steps, with isothermal intervals in between
- dynamic analysis, where temperature is changed in a continuous linear fashion

The analysis can be set up to end after a certain time, temperature or residual weight and be performed in vacuum, air or inert gas such as argon.

This analysis technique can be used to reveal many important temperature values where physical transformations or chemical reactions occur, pinpoint the presence of certain materials with known transition points, in samples of unknown composition, (e.g residual moisture can be detected by checking any sudden weight changes around 100 $°C$, water's boiling point), determine the complete degradation cycle of a sample, testing the thermal stability of a material at its operational temperature, etc.

The analysis has been firstly performed on the raw pellet material, as a benchmark test that consistently returned the expected degradation behaviour, over multiple analysis.
The test has then been conducted on powder samples and SLS printed samples, focusing on finding relevant discrepancies with the reference behaviour, which could potentially highlight the presence of impurities that might be undetectable by visual inspection of SEM images (showcased in section 11.1).

The TGA analysis was performed on a *Mettler-Toledo TGA/SDTA 851e* instrument (seen in Figure 10), in air atmosphere, with a heating rate of 10 $°C/min$ and a temperature range of 25 $°C$ to 900 $°C$.

Figure 10: Mettler-Toledo TGA/SDTA 851e

The specimens that have undergone a TGA analysis have been assigned an ID with the following criterion:

$$ID = xTGA_{NN} \tag{5}$$

where x is the specimen type (granule, powder or sintered), and NN is the sample number.

The specimens have been catalogued in table 1:

Table 1: TGA specimens

ID	Type
$gTGA_{01}$	pellet
$pTGA_{02}$	powder
$pTGA_{03}$	powder
$sTGA_{04}$	sintered

9.3 Density analysis

The true density of the powder is an important parameter to determine its flowability, which is a key factor in the SLS printing process, as better described in chapter 9.4.

Its value should be ideally identical to the theoretical density of the material, which is stated to be 1.20 kg/m^3 in its datasheet.

The density of the powder has been measured with a *Ultrapyc 5000 gas pycnometer*, as reported by Figure 11.

Figure 11: Ultrapyc 5000 gas pycnometer

A 0.626 g sample of the powder has been weighed and placed in the sample cell, then the pycnometer has been filled with helium gas and the measurements have been performed at 20 $°C$, using the *pulse* preparation and the *fine powder* flow rate presets available in the device settings.

The test has been iterated with a total of 15 steps, with a 0.01% precision and three measurements per pass, giving an average density value of 1.213602 kg/m^3, consistent with the expected theoretical value.

9.4 Flowability analysis

The flowability of a powder is a key factor in the success of the SLS process, as it impacts the way the powder is deposited on the build platform. Some powders are more prone to clumping, which can lead to the formation of bridges between the powder particles, which can cause the build platform to become clogged and the build to fail.

A powder with a good flowability will be able to flow freely and evenly, without clumping, and will be able to fill the build platform evenly, without leaving any gaps.

Powders with poor flowability can be improved by adding a flowability agent, which can be a lubricant, a binder or a combination of both.

The flowability of a powder can be tested by performing a flowability analysis, which can be performed in a number of ways, depending on the standard that is being followed.

The analysis has been performed on the powder samples, using the *tap density* method, which is the most common approximation test, as described by ASTM D7481 [23].

The standard describes how to evaluate the packing factor and the Hausner Ratio of a powder sample (that needs to be dried, before being tested, as residual moisture negatively impacts the flowability), using a 100 mL graduated cylinder, following the steps described for procedure *b*.

The Hausner Ratio is evaluated with equation 1, already described in previous chapters, and the packing factor is evaluated with equation 6:

$$\varphi = \frac{\rho_{bulk}}{\rho} \tag{6}$$

where ρ_{bulk} is the bulk density and ρ is the true material density.

As previously mentioned and according to the available literature, the Hausner Ratio of the powder should be ideally below 1.4 [9], which is consistent with the experimental findings.

9.5 Granulometry analysis

The granulometry analysis has been performed on an oven dried powder sample, using a *Malvern Morphologi 4*.

Figure 12: Malvern Morphologi 4

The sample has been measured in terms of volume, with a 5 mm^3 specimen being spread on a glass plate in the most homogeneous way possible, by using a 4 bar dispersion pressure and a 10 ms injection time.

An homogenous powder distribution is crucial in order to avoid particle overlap and to obtain a more accurate representation of the powder granulometry.

The instrument has taken several images of the powder specimen, using a 10X magnification, and by z-stacking images with different focal lenghts, in order to achieve better results.

All particles below 20 μm have been excluded from the analysis, which has been performed by using an automated static imaging algorithm, performed by the instrument's software.

10 3D printing

After the successful powder production (a typical batch is showcased in Figure 13), the next step was to print it with the SLS machine.

Before being printed, the powder could have been mixed with a small quantity of a binder, to improve its flowability. However, given the excellent flowability of the fine powder, this step has been skipped.

The next preparation step was to oven dry the powder again, in order to remove any residual moisture that could have accumulated during the storage period, and to homogenize the powder distribution by shaking the container for a few minutes.

Figure 13: SLS ready powder batch

10.1 Print files preparation

The following step was to prepare the print files, which are the files that have been sent to the SLS machine, to instruct it on how to print the parts.

The approach can vary depending on the software used to prepare the files, but the general idea is to create a 3D model of the part, then slice it into layers, and finally export the files to the SLS machine.

The pipeline started with the creation of a 3D model of the part and ended with a g-code file, and can be summarized as shown in Figure 14:

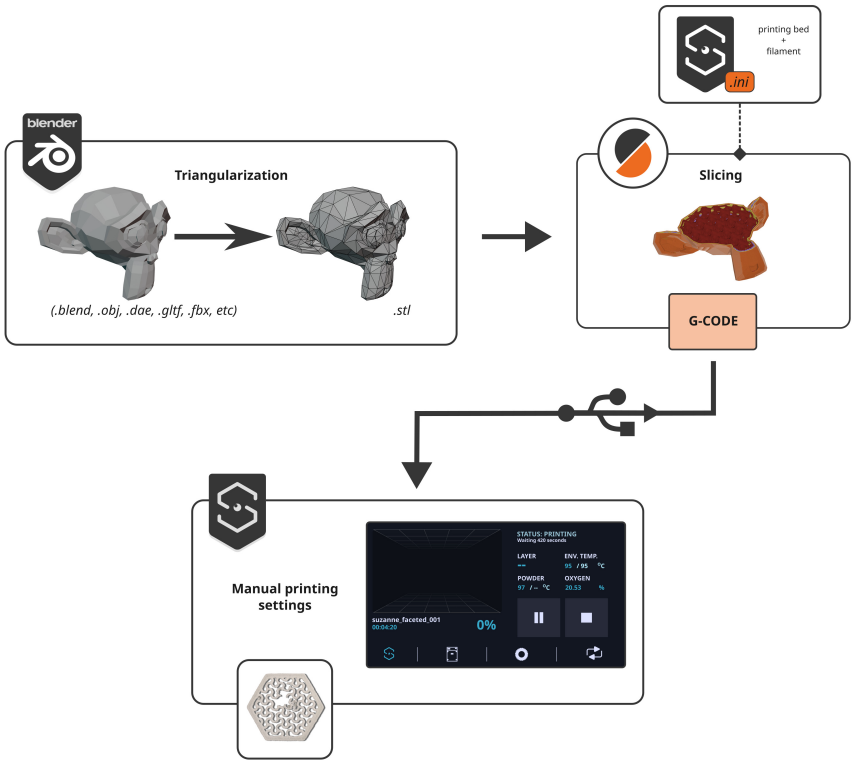

Figure 14: 3D printing file pipeline

10.1.1 3D model creation

The first step was to create a 3D model of the part, which can be done in many ways, depending on the software used.

The models have been created from scratch, either by directly modeling them in *Blender* 3.3.1, or by creating SVG files in *Inkscape* 1.2 and then extruding them in *Blender*, where they are handled as bezier curves.

This approach was particularly useful for this thesis work, where planar complex geometries better suit the SLS printing process with low powder availability and low printing volumes. As seen in section 11.5, the SLS printed parts are extremely small, with heights in the order of millimeters.

Working with planar geometries also allowed to easily create very intricate 3D models, by simply extruding the 2D SVG files, which as earlier mentioned are handled by Blender as a collection of bezier curves and thus the model inherits their properties, such as resolution dependant smoothness, non destructive ex-

trusion and custom profile beveling.

The extruded bezier curves have then been converted to meshes, remeshed when necessary, and finally exported as STL files (which is the most common file format for 3D printing), using Blender's internal 3D Printing Toolbox addon, which also offers useful mesh stats and automatic mesh fixing tools.

10.1.2 Slicing

The next step was to slice the 3D model into layers, which is handled by a general purpose slicing software.

The slicing software takes the STL file as input (or other formats such as OBJ, which are automatically triangulated during the import), and outputs a g-code file, which is the file that will be sent to the SLS machine.

There are some caveats with slicing software, which are worth mentioning.

The first one is that the software is not able to handle meshes with non manifold edges, so the STL file must be checked for non manifold edges before being imported.

More importantly, all slicing software is designed to work with an FDM workflow, whereas many industrial SLS machines tend to have a dedicated CNC software.
This means that the slicing software is not able to handle the SLS workflow without workarounds.
The most common workaround is to load a custom configuration file for the slicing software, which will instruct it on how to handle the SLS workflow for a specific printer. The slicing software is not aware of the SLS workflow, so it will slice the model based on a FDM workflow, and the custom configuration file, which bundles a set of parameters for the printing area and a fictitious filament.

While clearly there is no filament extrusion in SLS, once the software has sliced the model by simulating an FDM workflow, the output g-code file will be compatible with the SLS machine and provide accurate movement instruction.

The slicing software used for this thesis is *PrusaSlicer*, which is a free and open source slicing software, forked from the *Slic3r* project.

The SLS machine used for this case study does not have a dedicated CNC software, but the manufacturer provided a custom *.ini* bundle configuration file for *PrusaSlicer*, which is a universal file format, and can be used by any other slicing software as well.

10.2 Sharebot Snowhite²

The SLS machine used for this thesis is the *Sharebot Snowwhite²* (showcased in Figure 15), which is an open hardware and open source desktop SLS machine, designed by the italian company *Sharebot S.r.l.*.

Figure 15: Sharebot Snowhite²

The system is very modular and it features a standard powder distributor with a working area of 100x100x100 mm, but a reduced distributor with a 20x40x60 mm area has been used, given the available quantity of PHBH powder.

The printer utilizes a CO2 laser with a 14 W maximum power output and a 10.6 µm wavelength. Power is controlled as a percentage of its maximum output.
A value of 25 % has been generally set for solid pieces, whereas a 30-35 % range was preferred for pieces with extremely thin walls and intricate structures. The power for the border has been set to a 5 % relative increment, with respect to that used for the inner layers.

The printer features a user friendly touch screen GUI, but all its features and

logs can be accessed remotely for further control from any terminal.
The device is equipped with a 3D camera, which allows to monitor the printing process in real time, and to take pictures of the printed parts at every layer.

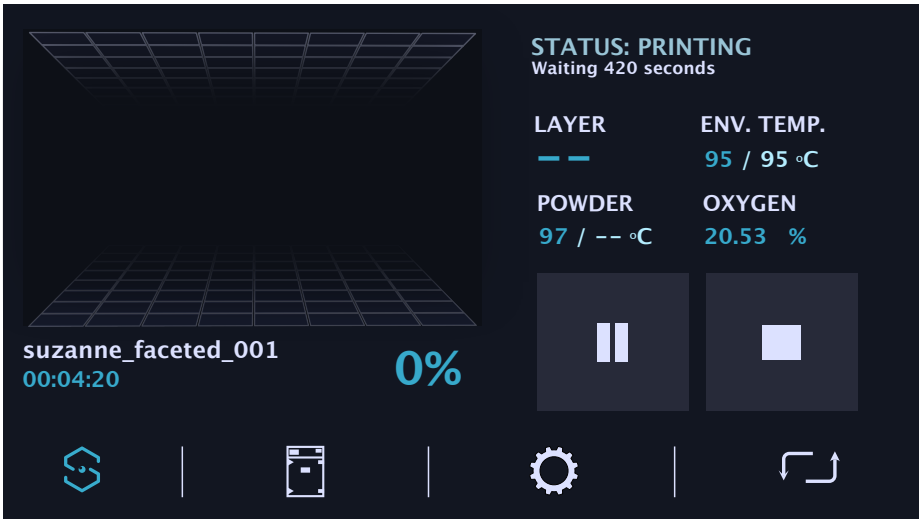

Figure 16: Sharebot Snowhite² UI

The polymer powder is generally distributed by the default blade recoater, but a roller option is also available. Air has been used for the printing process, but nitrogen or argon could be fed through the chamber, should a modified atmosphere be needed.

The printer is also equipped with a powder recovery system, which allows to recover the powder after the printing process, and to reuse it for further prints.

The environment temperature has been set in a range of 85-95 $°C$, with variable rates of success, whereas values outside this threshold showcased critical issues, i.e. high porosity, sheeting and delamination at low temperatures or adhesion to the recoater and consequent destruction of the printed specimen.

Another configurable variable is laser hatching speed, which is measured relative to machine resolution, in dots/s, which corresponds to 0.06 mm/s in metric units.
This has generally been kept at default values (40000 dots/s for the inner layers and 64000 dots/s for the border).

A maximum of three warming layers has been used for these prints, i.e. the powder is raised and warmed up for three layers, without any laser hatching, to allow the powder to settle and to avoid powder sheeting.

A higher number of warming layers might be needed for larger prints, but it has not been tested.

Once the environment temperature has been set in the desired range (ideally within the theoretical sintering window), the printer ramps it up in gradual steps, until the target is reached. An additional waiting time of 120-300 s has been set after reaching the desired temperature, in order to let heat uniformly distribute through the powder bed.

The tank offset has been set prior to printing, depending on the desired print height or layer number, which is calculated with the following formula:

$$Z = \frac{1}{2} \cdot (0.3\ N) \qquad [mm] \tag{7}$$

where:

- Z is the tank offset, in mm
- N is the number of layers to be printed
- 0.3 is the layer height, in mm, which is the default value for the *Sharebot Snowhite*[2]
- $\frac{1}{2}$ is a correction factor, which is needed to account for the fact that the printing area is fed powder from two side tanks.

As earlier mentioned, the printer is modular and despite being equipped with a default 100x100x100 mm working area, a reduced distributor with a 20x40x60 mm area has been used, given the available quantity of PHBH powder.

This setup is ideal for small scale prints, but as shown later, the current results are not exhaustively representative of the potential of the SLS workflow for PHBH.

There are in fact intrinsic limitations to extremely small objects with intricate and fine details, especially at low z-height, which are related to both the material itself (as it is fragile and prone to breaking) and the printing resolution of the SLS machine, which did not seem to be able to print extremely small features with high fidelity to the original models.

These limitations become less and less relevant with increasing z-height, as the part becomes more robust, as well as with increasing overall size, where the printing resolution is able to catch finer details with better accuracy.

Nonetheless, the current results are still very promising, and they showcase the potential of the SLS workflow for PHBH, which can be further explored with larger prints, where the complexity of the models can be pushed even further,

as expected with SLS technology.

The first samples were simple geometries, which have been printed to test the feasibility of the SLS workflow for PHBH. Square and rectangular prisms have been printed, with different z-heights, starting from single layers, up to 15 layers, as a baseline for the following tests.

The initial goal was in fact to find adequate printing parameters for the material, which required a lot of trial and error, as the material is very sensitive to the printing conditions.

The first prints have been made with a 25 % laser power setting, which has been found to be a reasonable value for solid pieces, by visual inspection of single layers (which showcased decent densification) and later confirmed by mechanical testing on multilayer samples.

As previously mentioned, the material is very sensitive to the printing conditions, and other than laser power, the environment temperature has been found to be the most critical parameter.

After a long series of tests, the optimal temperature range has been found to be 85 $^{\circ}C$ - 95 $^{\circ}C$, which has been used for the following tests.

It is important to note that the environment temperature is measured by a thermocouple, whereas the powder bed temperature (which is a few degrees higher) is measured by an infrared sensor, which is less accurate.
Therefore, these values might vary slightly for different machines, depending on how the different temperatures are measured.

The next step was to test the material with more complex geometries, which have been printed with the same temperature range, but with a 30-35 % laser power setting, which has been found to be optimal for the emptier geometries, where heat is dissipated more easily, given the lower thermal mass.

When dealing with thin, hollow and complex geometries, the most prominent issue is the tendency of the blade recoater to stick to the printed piece and wipe the part out, which is a common issue with SLS technology, and which can be caused by different factors, such as the powder bed temperature, the laser power, the environment temperature, the powder type and the powder distribution, among the many.

Given the multifactorial and complex nature of the aforementioned issue, it is not possible to pinpoint the exact cause of the problem, but finding a compromise between the different parameters proved to be a viable and practical option, which allowed for successful prints.

The introduction of other settings such as warming layers, pre-print and between-layers waiting time, has been found to be useful in order to avoid the blade recoater from wiping the part out.

Using a roller recoater might also be a viable solution, but it has not been tested.

The following printed specimens have been modeled as previously mentioned and have been catalogued in table 2 with the following criterion:

$$NN - SLS_{MM} \tag{8}$$

where:
NN is the number of layers and MM is the sequential number of the sample, respectively.

Table 2: A list of the most relevant 3D printed specimens

ID	*Layers*	*Laser power [%]*	*Environment temperature [°C]*
$15 - SLS_{01}$	15	25	90
$15 - SLS_{02}$	15	25	95
$55 - SLS_{03}$	55	35	95
$01 - SLS_{04}$	01	25	85
$50 - SLS_{05}$	50	30	90
$10 - SLS_{06}$	10	25	90
$15 - SLS_{07}$	15	25	90
$15 - SLS_{08}$	15	35	87

10.3 Dynamic Mechanical Analysis (DMA)

A non-destructive DMA has been used to determine some of the mechanical properties of SLS printed PHBH. The analysis allows for the determination of the storage modulus E', the loss modulus E'' as well as the tanδ, which is the ratio between the loss modulus and the storage modulus.

As mentioned in chapter 9.2.1, the DMA can also be used to better determine the glass transition temperature T_g [24], which has been initially estimated to be around 2 $°C$ by the DSC analysis of a PHBH powder sample, as visible in Figure 25. However, the revealed peak activity in that temperature range can not be attributed to the glass transition in a definitive way, by means of a DSC analysis alone.

The glass transition temperature, which is defined as the temperature at which the material changes from a glassy to a rubbery state, (i.e. the temperature at which the material changes its stress-strain behavior from brittle to plastic), can be determined with better precision by a DMA.

More specifically, the transition point can be revealed by a prominent peak in the tanδ curve, indicating a sudden change in the moduli ratio of the material.

The analysis has been performed with a Triton Technology DMA instrument, on the SLS sample $10-SLS_{06}$ that has been printed specifically for the purpose of the DMA analysis.

The test has been run with an oscillating uniaxial stress amplitude of 1 N, at a frequency of 1 Hz, with an initial chamber temperature of -77.7 $°C$ (achieved by cooling the environment with liquid nitrogen), and has been stopped once the sample reached the rubbery plateau, i.e. a temperature region below the melting point, in which the material exhibits an almost constant modulus behaviour [25].

11 Analyses results

Given the wide variety of instruments and their vastly different release date, the various included software suites and operating systems involved, all the different output files have been analyzed and uniformed as tab separated values UTF-8 text, using standard unix cli tools.

The uniforming of datasets later favoured the data analysis workflow, which has been performed by using *GNU Octave* and *Labplot*.

11.1 SEM Results

The FIB-SEM instrument has produced a total of 12 different images, the most relevant have been edited using *Pixelmator Pro* and *GIMP* and are shown below:

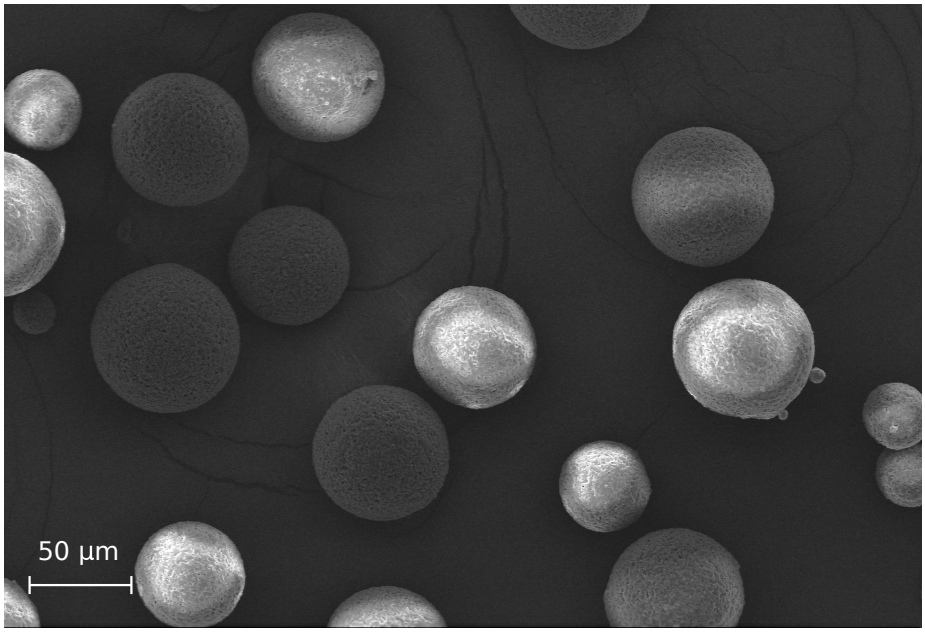

Figure 17: Enhanced SEM image, SEM_{02} with a 461X magnification factor

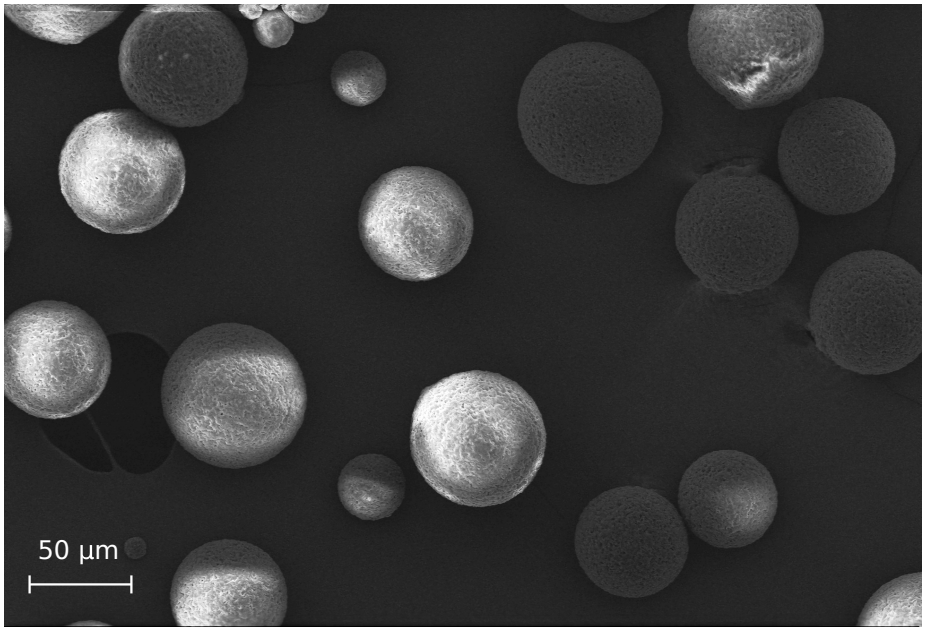

Figure 18: Enhanced SEM image, SEM_{03} with a 461X magnification factor

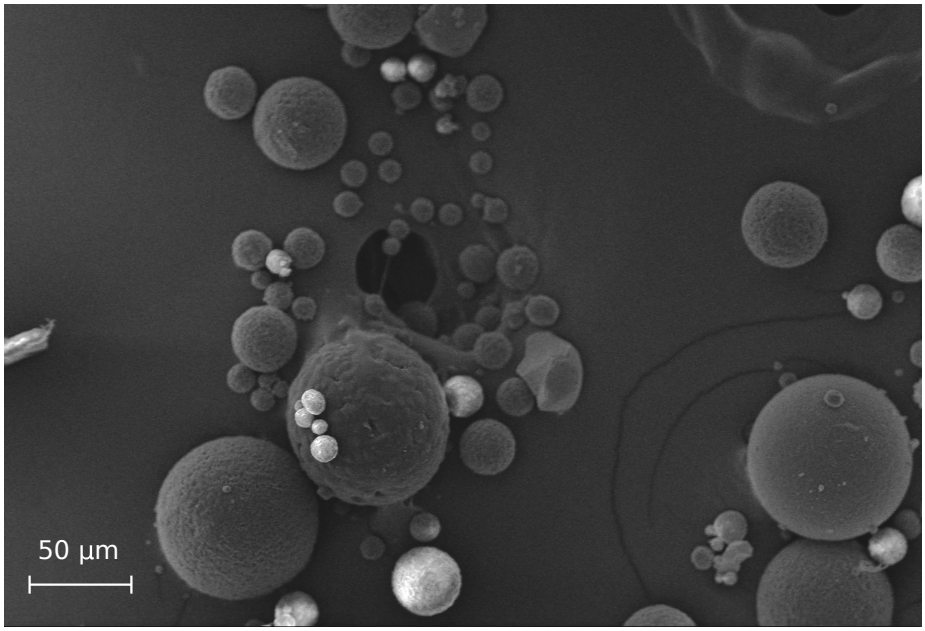

Figure 19: Enhanced SEM image, SEM_{05} with a 461X magnification factor

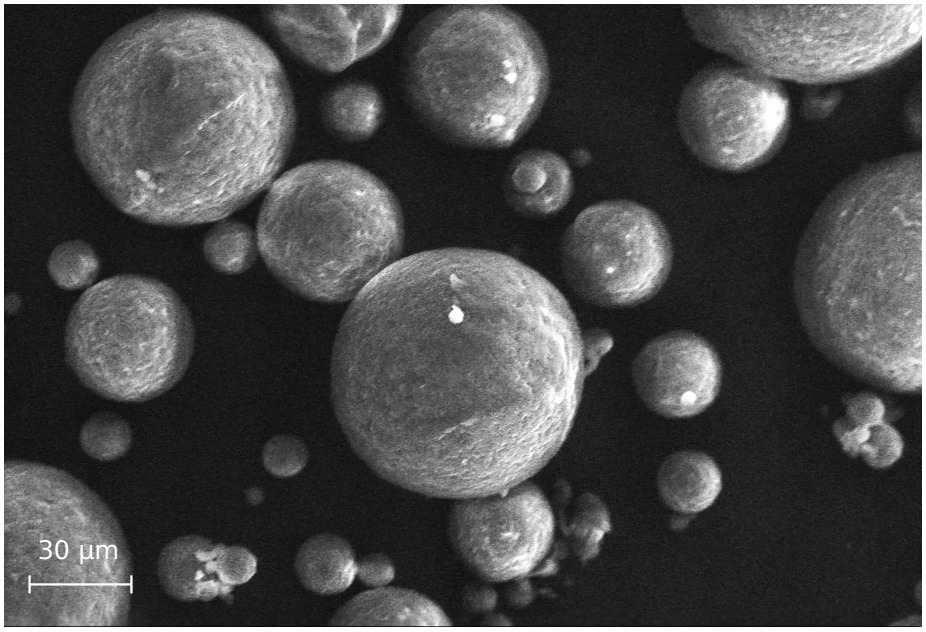

Figure 20: Enhanced SEM image, SEM_{08} with an 800X magnification factor

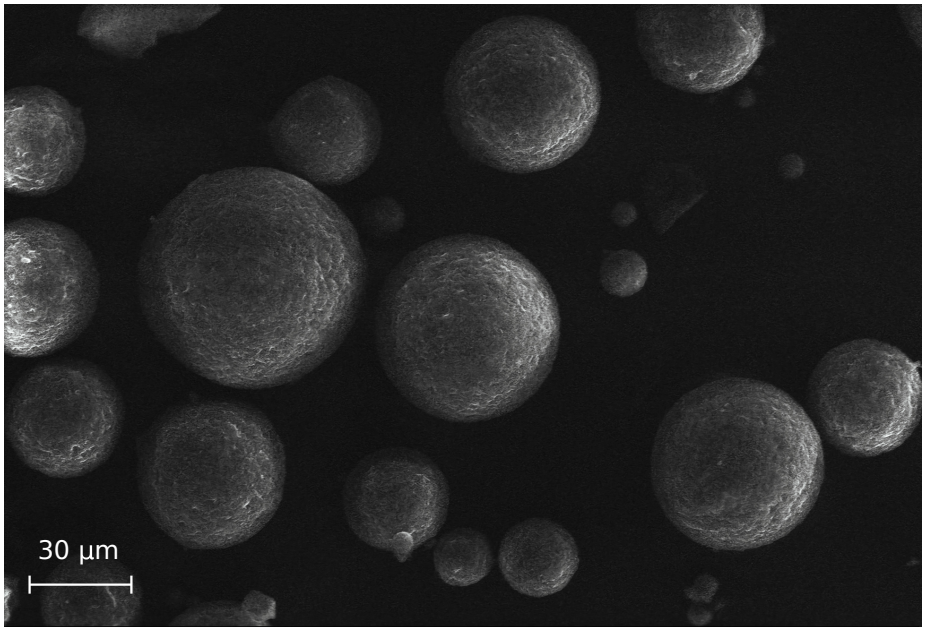

Figure 21: Enhanced SEM image, SEM_{09} with an 800X magnification factor

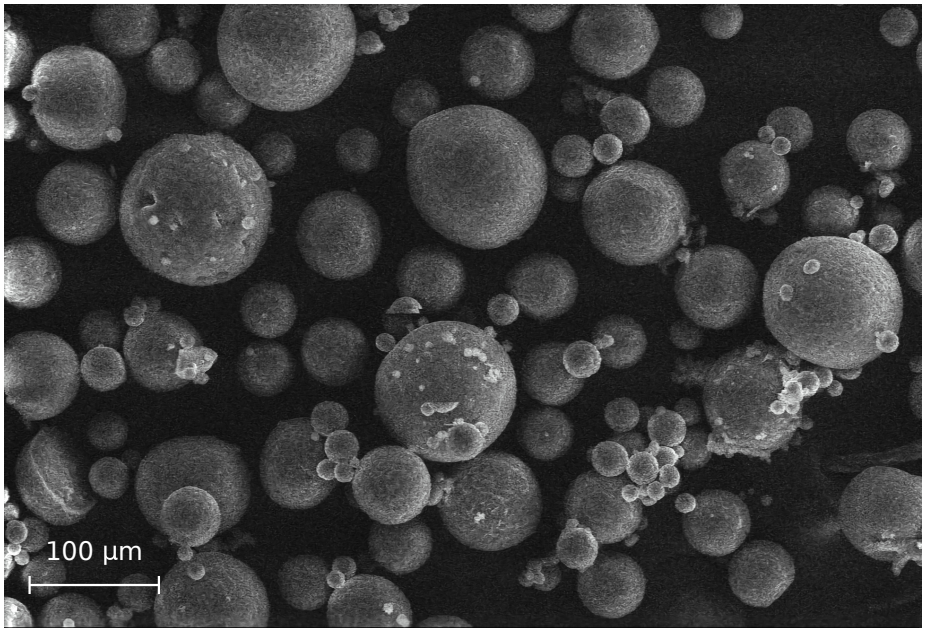

Figure 22: Enhanced SEM image, SEM_{12} with a 400X magnification factor

11.2 Granulometry Results

The output data has been analyzed and the most meaningful features have been plotted as vector images using *Labplot* and postprocessed with *Inkscape*.

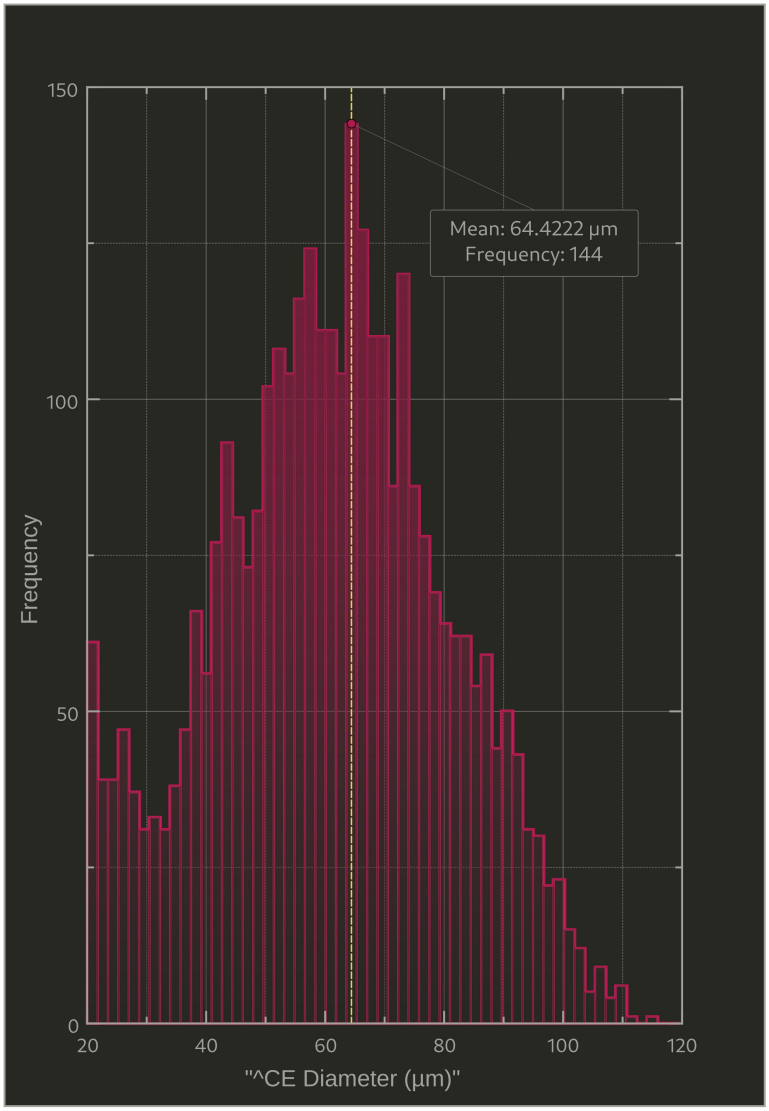

Figure 23: Particle Size Distribution of a powder sample

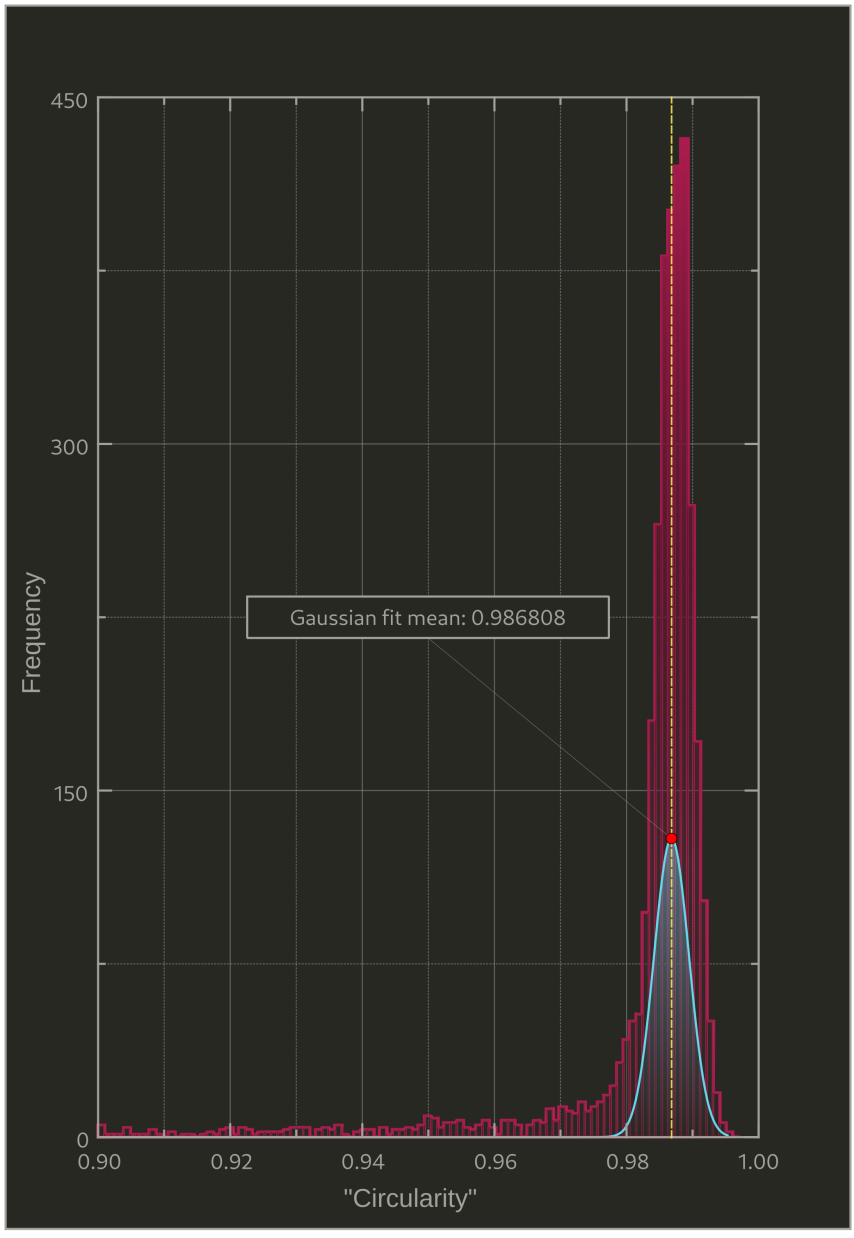

Figure 24: Particle Circularity Distribution of a powder sample

The results of the granulometry analysis showcase particle sizes compatible with SLS powder requirements emphasized in previous sections, as well as a great particle circularity distribution, which is consistent with the findings of the SEM analysis reported in section 11.1.

The average particle diameter is 64.4222 μm, with a count of 144 over a total of more than 3000 analyzed particles, as shown in Figure 23.

The average circularity is extremely close to a perfectly spherical shape, with a mean value of roughly 0.98, as clearly visible in Figure 24.

11.3 DSC Results

The analysis results have been plotted using *Labplot* and *Inkscape*, using the *exo-up* convention, with the raw pellet curves used as a baseline for the powder curves.

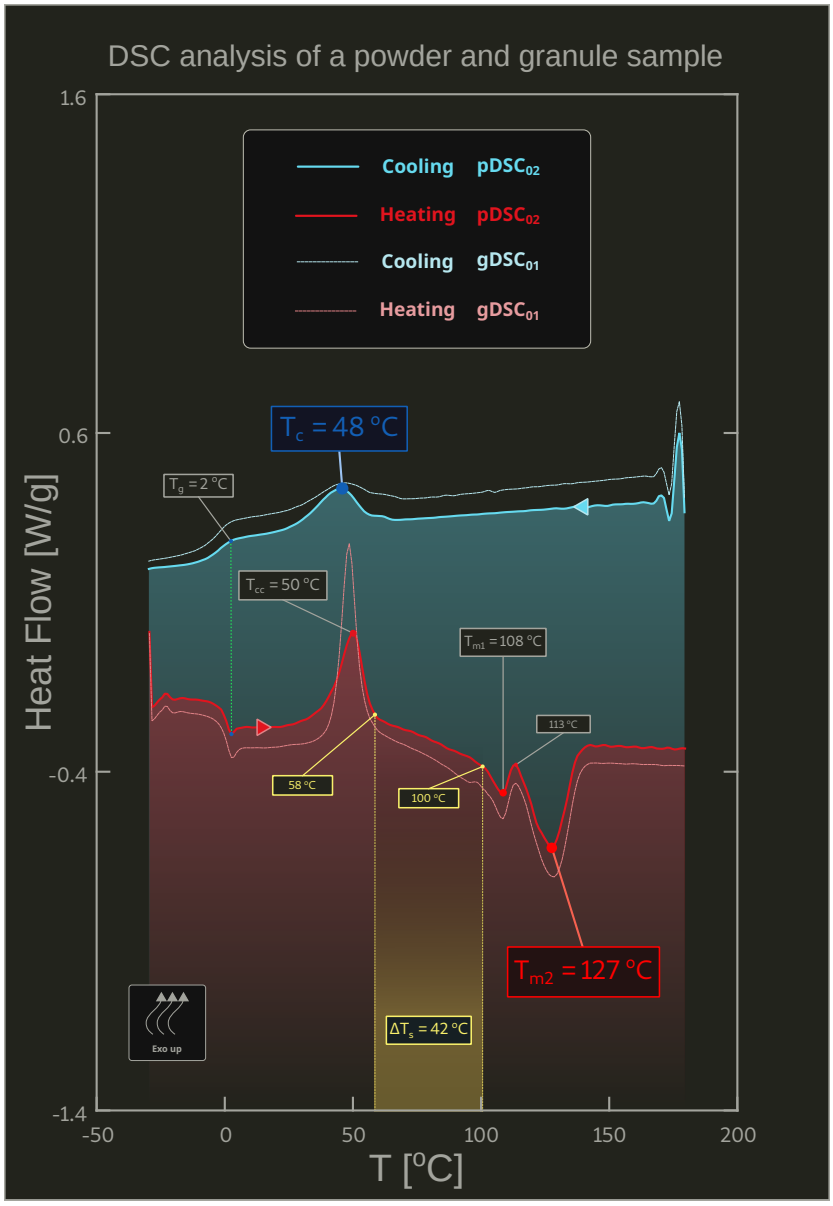

Figure 25: DSC analysis of PHBH at 10 $°C/min$, exo-up convention

The plot highlights a consistent behaviour and only minor differences between the powder and pellet samples, with the powder specimen showing a slightly wider sintering window, which is a very desirable trait for SLS, as explained in previous chapters and in accordance with the available literature [2, 9, 18].

As evident from the heating phase (visible in Figure 25), the powder sample shows a main peak melting point of $T_m = 127.164\ ^\circ C$, with a secondary melting point of $T_m = 108.164\ ^\circ C$, as well as a crystallization point at $T_c = 50.1643\ ^\circ C$. The cooling phase highlights a main peak crystallization point of $T_c = 48.254\ ^\circ C$ as well, indicating that the main crystallization activity occurs around that temperature range in both phases.

A minor peak activity is also observed at around $2\ ^\circ C$ in both the heating and cooling phases (with a more prominent peak during heating), and this can be attributed to the glass transition temperature of the polymer, which can be further investigated using a DMA, as documented in section 10.3.

The powder sample data has been used to calculate the enthalpy values around the two main crystallization peaks and the main melting peak, with the following approach:

- The heat flow data points are normalized by the specimen weight, which does not have a data set of its own from the DSC test, but can be assumed to be constant within the temperature range, which is a resonable assumption based on the TGA results
- The normalized heat flow is then plotted against time for both the heating and cooling phases and a line is hand drawn around the peaks
- The area between the peaks and the base line represents an estimate of the enthalpy value

The enthalpy values, extrapolated from Figure 26, are then calculated using the integral equation 9, which is solved numerically:

$$\Delta H = \int_{t_0}^{t_1} \phi(t)\, dt \quad [J/g] \tag{9}$$

where $\phi(t)$ is the normalized heat flow and t_0 and t_1 are the time values at which the line is drawn.

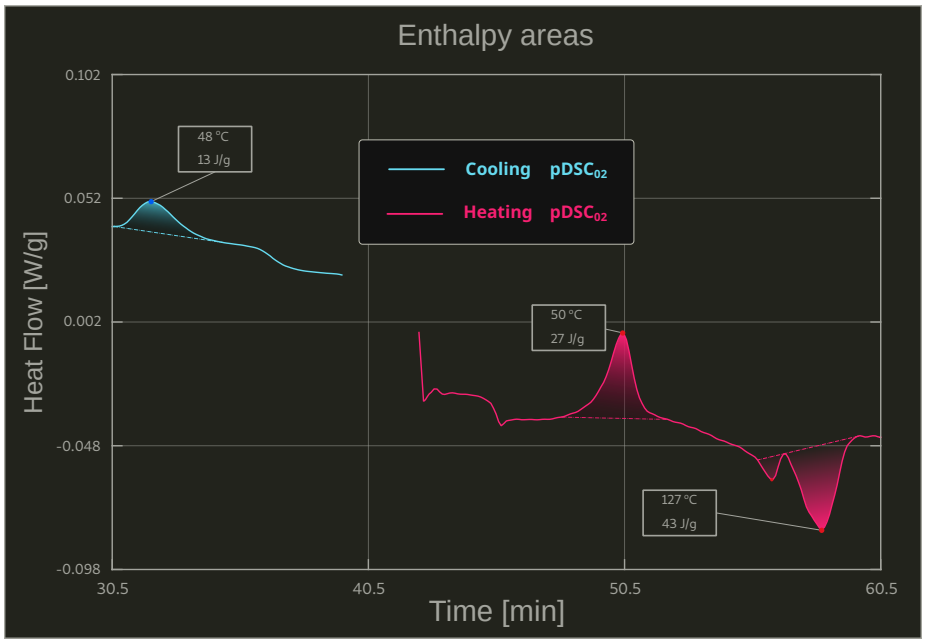

Figure 26: Enthalpy values for the DSC analysis of PHBH at 10 $°C/min$

The obtained enthalpy values can be used to derive the estimated percentage of crystallinity of the material, using the following equation:

$$X_c = \frac{\Delta H_m - \Delta H_{cc}}{\Delta H_m^0 \cdot m} \quad [\%] \tag{10}$$

where ΔH_m is the enthalpy value of the melting peak, ΔH_{cc} is the enthalpy value of the cold crystallization peak, m is the mass of the specimen and ΔH_m^0 is the enthalpy value of the melting peak of a pure crystalline material, which is 146 J/g for PHBH [26].

All the highlighted temperatures and other relevant quantities are summarized in table 3:

Table 3: Results of the DSC analysis showcasing phase transition points, enthalpies and crystallinity of the material

ID	ΔH_c $[J/g]$	T_c^p $[°C]$	T_g $[°C]$	T_{cc}^p $[°C]$	ΔH_{cc} $[J/g]$	ΔH_m $[J/g]$	T_{m1}^o $[°C]$	T_{m1}^p $[°C]$	T_{m2}^o $[°C]$	T_{m2}^p $[°C]$	X_c [%]
gDSC	11	49	2	49	36	49	103	108	111	129	11
pDSC	13	48	2	50	27	43	100	108	113	127	15

11.4 TGA Results

The analysis data has been exported with *Mettler-Toledo*'s included software, after normalizing the data to the initial weight of the sample, then uniformed to the rest of the datasets and imported, elaborated and plotted with *Labplot*.

The following Figures 27, 28 show the results of the TGA analysis on the pellet and powder sample, respectively.

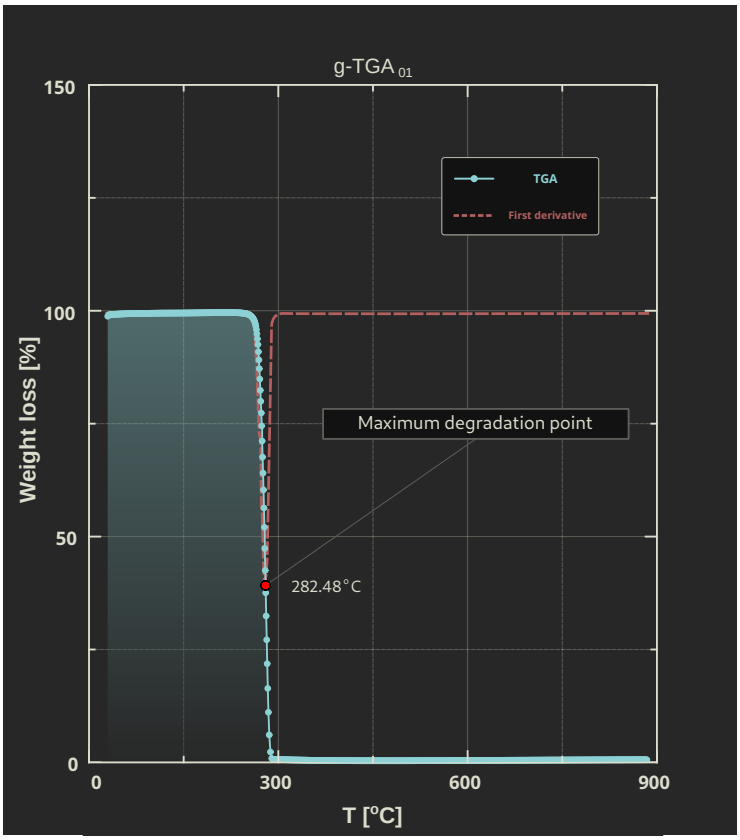

Figure 27: TGA analysis of pellet sample $gTGA_{01}$ (as in table 1)

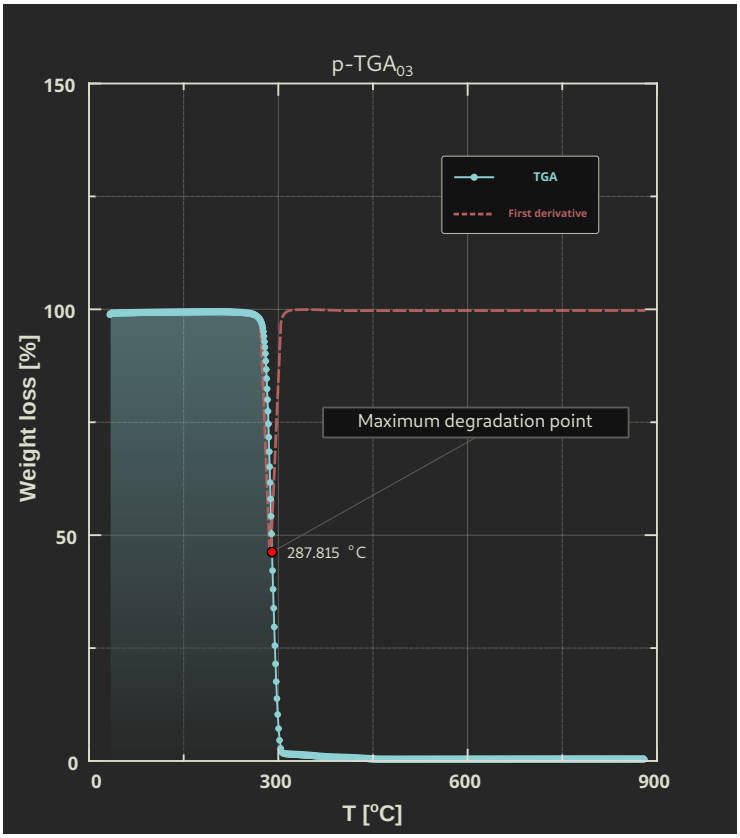

Figure 28: TGA analysis of powder sample $pTGA_{03}$ (as in table 1)

The results of the TGA analysis showcase the expected thermal behaviour of the powder and sintered samples, which are consistent with the pellet sample.

The TGA curves show an exponentially incresing weight loss, with very similar slopes, and the additional first derivative showcases a consistent behaviour among all samples, with clear degradation peaks at approximately the same temperature values.

The consistent behaviour between the raw material and the obtained powder is also showcased in Figure 29, where the overlap of the curves is abundantly clear.

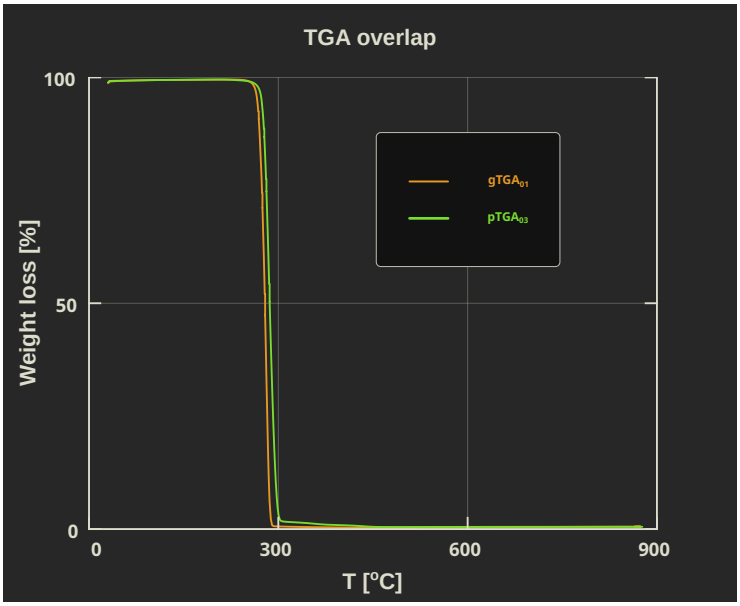

Figure 29: TGA curves of both the raw material and the obtained powder overlapped

The results are already very promising, as no significant sign of degradation is observed at the temperatures of interest, which is the range comprised by the sintering window, previously identified in the DSC analysis.

11.5 3D Printing Results

Given the experimental nature of this work, several samples have been printed, with gradual increases in complexity, in order to test the limits of the SLS workflow for the novel material.

The printed parts showcase an excellent level of detail, which could potentially increase when printing larger objects. Other than some superficial roughness and bumps, which are expected in most AM before surface treatments, the specimens are in a very good condition, with no visible cracks or other defects.

The most significant specimens have been cut out from their photos and put against a pitch black background using *Pixelmator Pro*, then assigned a size marker using *Inkscape*, as showcased in Figures 30 to 34:

Figure 30: DMA ready prismatic specimens $10-SLS_{06}$ (bottom) and $15-SLS_{07}$ (top).

Figure 30 shows the two prismatic specimens intended to be used for DMA testing. As a result of multiple printing attempts, using filled geometries with an increasing number of layers, both the 10 and 15 layers specimens have been successfully printed with a 25 % laser power at a 90 $^{\circ}C$ environment temperature.

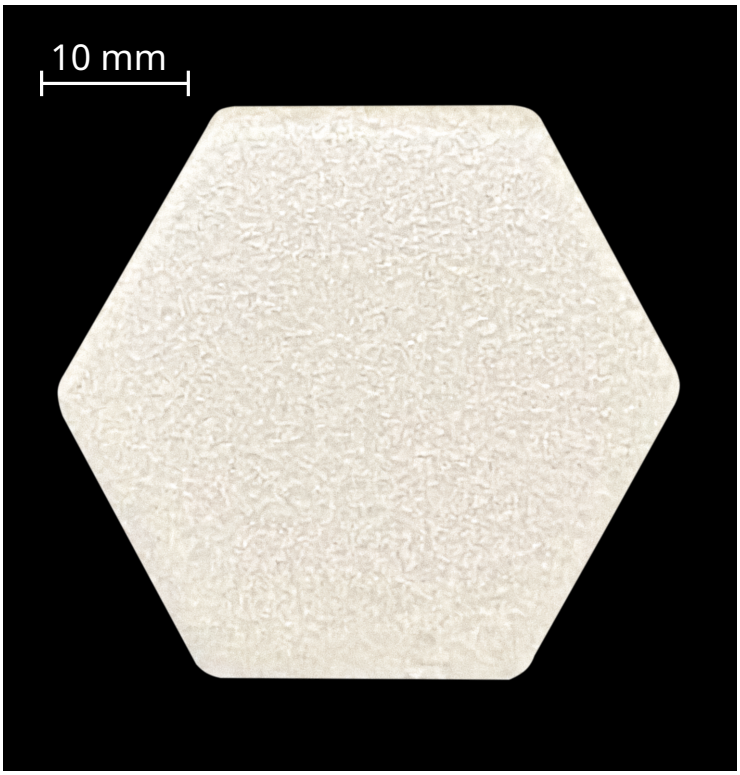

Figure 31: Specimen $15 - SLS_{02}$, a filled hexagon.

The shape in Figure 31 is a 15 layer filled hexagon, which has been printed with a 25 % laser power at a 95 $°C$ environment temperature.
The specimen was printed to test a more complex shape than a prism, with the same number of layers, as well as to test the effect of a higher environment temperature on the printing process, which remained stable in the range of 90-95 $°C$, for filled geometries and a 25 % laser power.

The stabilization of the printing process for filled parts of simple shapes, launched the idea of printing more complex shapes, with internal patterns, curvatures and holes.

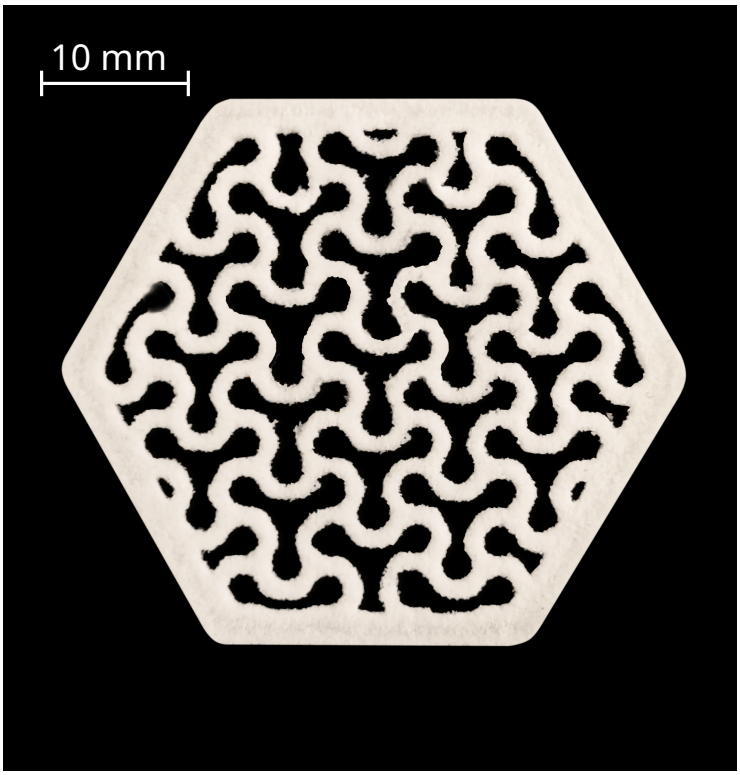

Figure 32: Specimen $15 - SLS_{08}$, showcasing a complex internal pattern.

The organic pattern showcased in the 15 layers specimen in Figure 32 has been printed with a 35 % laser power, at a slightly lower 87 $^{\circ}C$ environment temperature, which has resulted in a rougher surface. However, the higher laser power has allowed for a more intricate pattern to be printed, since attempts with a 25 % value resulted in a very poor quality print, in configurations with thin walls.

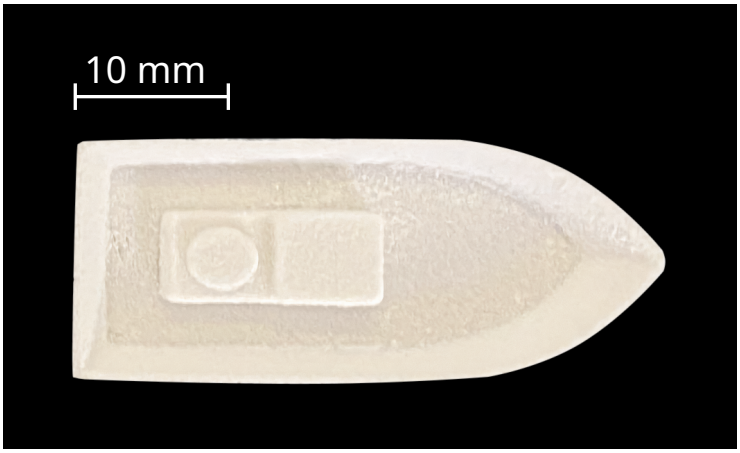

Figure 33: Specimen $50 - SLS_{05}$, representing a boat model with curvatures.

The boat in Figure 33 has been printed with a slightly lower 30 % laser power, at a 90 $^{\circ}C$ environment temperature. This was the first specimen to reach a 50 layer thickness, after several attempts. Despite being filled, the specimen has a curved thin wall, which was more challenging to print.

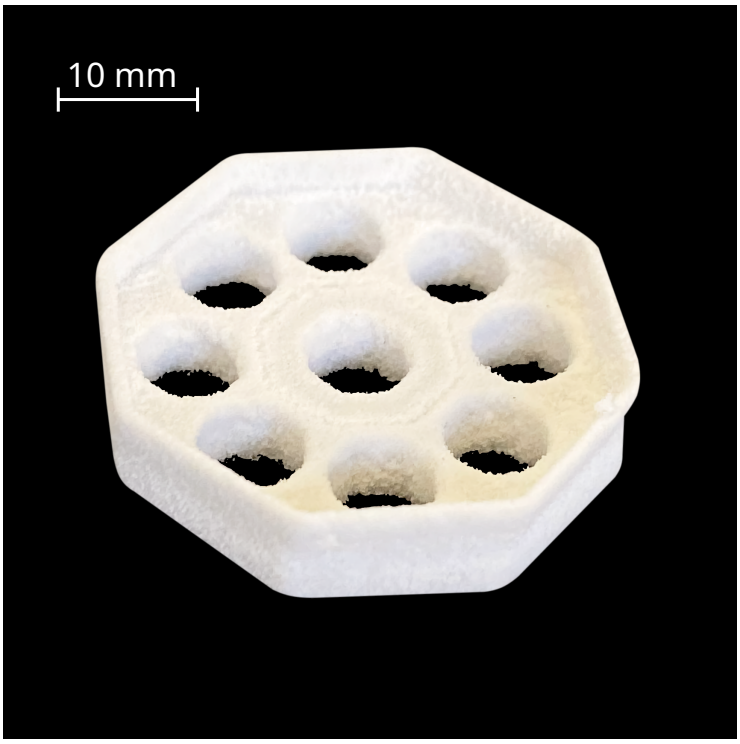

Figure 34: Specimen $55 - SLS_{03}$, an octagon with a circular array of octagonal holes and a thin wall rim, with a total height of 55 layers.

Last but not least, the octagonal specimen in Figure 34 was the first to reach a 55 layer thickness, as well as the first to showcase a thin wall rim, an internal array of octagonal holes and extremely small indentations at the same time. This specimen has been printed with a 35 % laser power at a 95 $°C$ environment temperature. The higher power was necessary to print the thin wall rim, while the higher temperature was necessary since the rest of the specimen is mostly filled on the inside.

11.5.1 Thermal stability

As a further testimony of the consistent thermal behaviour of the biopolymer along the entire pipeline, the overlap of the TGA curves of the pellet, powder and sintered samples is shown in Figure 35:

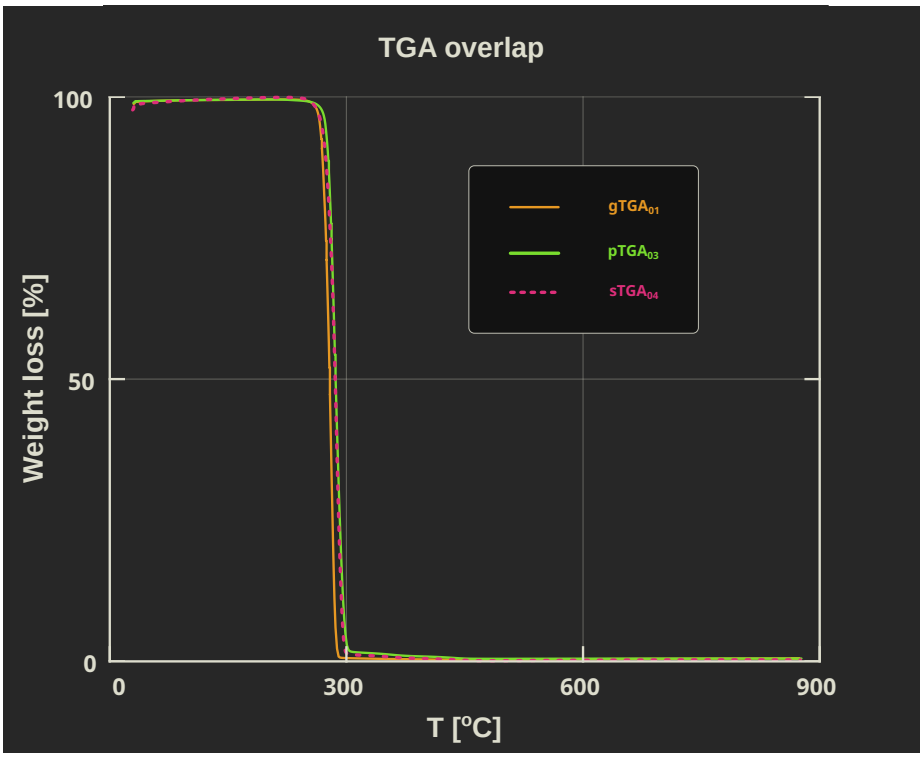

Figure 35: Consistent results of the TGA analysis of the pellet, powder and sintered samples

11.5.2 DMA Results

The results of the DMA analysis are shown in Figure 36, where the tanδ curve has been upscaled significantly in order to match a relative scale with the other curves.

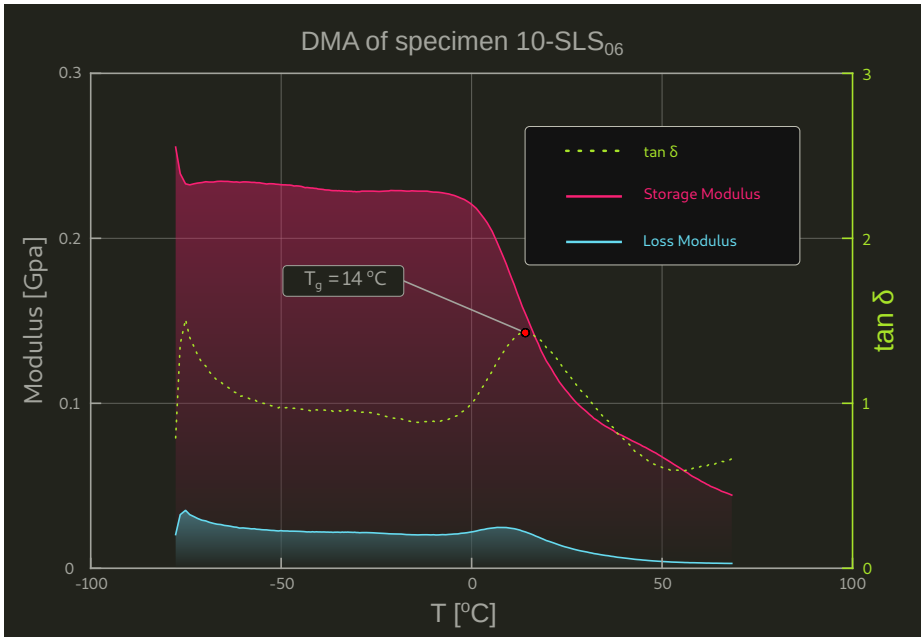

Figure 36: DMA analysis of sample $10 - SLS_{06}$ (as reported in table 2).

The tanδ curve visible in Figure 36 shows a clear peak at 14.1 $°C$, which is the glass transition temperature of the material, in disaccordance with the initial estimation of 2 $°C$ (as seen in Figure 25).

As expected for a polymer of the PHA family, both the storage modulus E' and the loss modulus E'' are very low, in line with the typical viscoelastic behavior of all bio-based polymers [11, 27], which are not suited for structural applications and are instead used for packaging [14] and other non-structural applications, such as biomedical implants and scaffolds [8, 28].

Unsurprisingly, the mechanical properties of the material fall behind those of typical SLS polymers [13], which can occasionally reach storage moduli a whole order of magnitude higher than that of PHBH [29].

That in itself is not a major issue, as SLS parts are not limited to structural applications or mechanical pieces: other properties, such as biodegradability,

biocompatibility and low toxicity can be very desirable traits in a wide range of applications [10, 11].

Moreover, the mechanical and thermal properties of the material can be improved by adding fillers, creating blends with other bio-based polymers or creating composites with other materials [4, 18, 26, 30–32].

Given the successful SLS printability, with unaltered thermal properties among the raw material, the powder and the printed parts (as highlighted by the TGA and DSC analysis results), as well as mechanical properties that meet the expected behavior of a bioplastic, PHBH is a very promising bio-based polymer that can further enrich the catalogue of sustainable materials available for additive manufacturing.

12 Conclusions

The aim of this work was to investigate the feasibility of PHBH as a material for additive manufacturing, with a particular focus on the SLS process.

The entire work has been very experimental and innovative in nature, as it is the first time that a novel bio-based polymer such as PHBH has been investigated for the aforementioned use and brought to the point of being printable with SLS.

The approach has been exploratory and yet successful in all of its phases, starting from the powder production and characterization, all the way to the successful SLS printing of the material, which leaves even more room for further research and development.

As stated and reiterated throughout the work, producing an SLS suitable powder with a novel material and no prior knowledge of the process is a very challenging task, which requires a lot of trial and error and a lot of patience. Despite the difficulties and the lack of a clear and straightforward blueprint for the precipitation reaction in the available literature, the powder was successfully produced and characterized, with an outstanding morphology and an adequate particle size distribution, and the pellet to powder yield being substantially higher than the initially expected results, which is a very positive outcome and a testament to the success of the production pipeline.

The highlight of the work is the successful SLS printing of the material, which has been achieved with no previous experience of the process with PHBH or any other bio-based polymers of similar characteristics. The printing process was very challenging and required a lot of manual tweaking and adjustments, based solely on the data obtained from the powder characterization and the experience with SLS printing of other materials [33].

The printing process was gradually explored: progressively more complex prints have been achieved by building upon the knowledge acquired from the previous iterations, starting with mono-layer prints of simple square sheets, then multi-layer filled pieces and finally ending with more intricate parts, up to a total height of 55 layers.

As a final step and further proof of the feasibility of the material for SLS printing, the PHBH printed parts have been analyzed with a DMA, which has shown that the material's mechanical properties are in line with those expected for bio-based polymers and, most importantly, that the thermal stability of the material is stable throughout the entire process, from the raw material all the way to the printed part, as assessed by the additional TGA in Figure 35.

13 Future development

The entire project has been carried out with an experimental approach and, despite poor direct support from the currently available literature, a better understanding of the material and its behavior has emerged, but the need for further research and development is still present.

Starting from the powder production pipeline, the results have already been excellent with the available notions and tools, bringing the pellet to powder yield to a very significant increase.

However, the process is still in its infancy, and the entire premise of the project is to develop a sustainable and cost-effective production pipeline, which is not only able to produce a high-quality powder, but also to do so in a way that is environmentally friendly. Therefore, the next step is to find a way to reproduce and even improve the results obtained with the current recipe, but in a more sustainable way, by further investigating the use of alternative solvents.

Another possibility is to find a way to retrieve the evaporated chloroform, assuming an effective solvent recovery system is available and cost-effective.

The next step is to further investigate the use of the powder in the SLS process, by further optimizing the printing parameters, the powder granulometry and morphology and experimenting with different additives or material blends that could improve the mechanical properties of the material, as well as investigating the possibility of enhancing the printed parts with post-processing techniques.

Bibliography

Articles

[1] ASTM. "Standard Guide for Nondestructive Examination of Metal Additively Manufactured Aerospace Parts After Build". In: (2020).

[2] Maximilian A Dechet and Jochen Schmidt. "On the Development of Polymer Particles for Laser Powder Bed Fusion via Precipitation". eng. In: *Procedia CIRP* 94 (2020), pp. 95–99. ISSN: 2212-8271.

[3] O. Semeniuta I. Baturynska and K. Martinsen. "Optimization of Process Parameters for Powder Bed Fusion Additive Manufacturing by Combination of Machine Learning and Finite Element Method: A Conceptual Framework". In: *Procedia CIRP* 67 (2018). DOI: 10.1016/j.procir.2017.12.204.

[4] Lisa Jiaying Tan; Wei Zhu; Kun Zhou. "Recent Progress on Polymer Materials for Additive Manufacturing". In: *Advanced Functional Materials* (2020).

[5] F.M. Abdullah A. Alfaify M. Saleh and A.M. Al-Ahmari. "Design for Additive Manufacturing: A Systematic Review". In: *Sustainability* 12 (2020). DOI: 10.3390/su12197936.

[6] A. Vevers; A. Kromanis; E. Gerins; J. Ozolins. "Additive Manufacturing and Casting Technology comparison: mechanical properties, productivity and cost benchmark". In: *Latvian Journal of Physics and Technical Sciences* (2018).

[7] Balachandramurthi Arun Ramanathan; Moverare Johan; Mahade Satyapal. "Additive Manufacturing of Alloy 718 via EBM: Effect of post-treatment on the microstructure and the mechanical properties". In: *Materials* (2019).

[8] Alberto Giubilini et al. "Advantages of Additive Manufacturing for Biomedical Applications of Polyhydroxyalkanoates". In: *Bioengineering* 8.2 (2021). ISSN: 2306-5354. DOI: 10.3390/bioengineering8020029.

[9] Manfred Schmid, Antonio Amado, and Konrad Wegener. "Polymer powders for selective laser sintering (SLS)". In: *AIP Conference Proceedings* 1664.1 (2015), p. 160009. DOI: 10.1063/1.4918516.

[10] T. Pan et al. "Selective laser sintering 3D printing of biomedical polymer materials". Chinese. In: *Gaofenzi Cailiao Kexue Yu Gongcheng/Polymeric Materials Science and Engineering* 32.3 (2016), pp. 178–183.

[11] Adriana Kovalcik. "Recent Advances in 3D Printing of Polyhydroxyalkanoates: A Review". In: *The EuroBiotech Journal* 5 (2021).

[13] Federico Lupone; Elisa Padovano; Francesco Casamento; Claudio Badini. "Process Phenomena and Material Properties in Selective Laser Sintering of Polymers: A Review". In: *Materials* (2021).

[14] Z.U. Arif M.Y. Khalid. "Novel biopolymer-based sustainable composites for food packaging applications: A narrative review". In: *Food Packaging and Shelf Life* 33 (2022). DOI: 10.1016/j.fpsl.2022.100892.

[15] D. Monticone R. Patel et al. "Hydrolytic degradation of porous poly(hydroxybutyrate-co-hydroxyvalerate) scaffolds manufactured using selective laser sintering". In: *Polym Degrad Stab* 187 (2021).

[16] KBV Research. "Global Additive Manufacturing Market Size, Share and Industry Trends Analysis Report by Printer Type, By Technology, By Component, By Application, By Material, By Vertical By Regional Outlook and Forecast". In: (2022).

[17] M. Erharter A. Xu B. Langefeld and V. Kourkejian. "Market, machines and materials – The new playground for large chemical companies". In: (2020).

[18] Kerim Eraslan et al. "Poly(3-hydroxybutyrate-co-3-hydroxyhexanoate) (PHBH): Synthesis, properties, and applications - A review". In: *European Polymer Journal* 167 (2022), p. 111044. ISSN: 0014-3057. DOI: 10.1016/j.eurpolymj.2022.111044.

[19] Gomez Bonilla; Dechet M.A.; Schmidt J.; Peukert W.; Buck A. "Thermal rounding of micron-sized polymer particles in a downer reactor: direct vs indirect heating". In: *Rapid Prototyping Journal* 26.9 (2020).

[20] Hemantkumar Junghare*; Mayur Hamjade; C.K.Patil; S.B.Girase; Mandar M.Lele. "A Review on Cryogenic Grinding". In: *International Journal of Current Engineering and Technology* (2017).

[21] M.A. Dechet et al. "Production of polyamide 11 microparticles for Additive Manufacturing by liquid-liquid phase separation and precipitation". In: *Chem Eng Sci* 197 (2019). DOI: 10.1016/j.ces.2018.11.051.

[22] Z. Asiedu J. Nikiema. "A review of the cost and effectiveness of solutions to address plastic pollution". In: *Environmental Science and Pollution Research* 29 (2022). DOI: 10.1007/s11356-021-18038-5.

[23] ASTM. "Standard Test Methods for Determining Loose and Tapped Bulk Densities of Powders using a Graduated Cylinder". en. In: ASTM D7481 18 (2018).

[24] C.A. Gracia-Fernández et al. "Comparative study of the dynamic glass transition temperature by DMA and TMDSC". In: *Polym Test* 29 (2010). DOI: 10.1016/j.polymertesting.2010.09.005.

[26] J. Ivorra-Martinez et al. "Development and characterization of sustainable composites from bacterial polyester poly(3-hydroxybutyrate-co-3-hydroxyhexanoate) and almond shell flour by reactive extrusion with oligomers of lactic acid". English. In: *Polymers* 12.5 (2020).

[27] Jian Zhang, Valerian Hirschberg, and Denis Rodrigue. "Mechanical fatigue of biodegradable polymers: A study on polylactic acid (PLA), polybutylene succinate (PBS) and polybutylene adipate terephthalate (PBAT)". In: *International Journal of Fatigue* 159 (2022), p. 106798. ISSN: 0142-1123. DOI: 10.1016/j.ijfatigue.2022.106798.

[28] A. Kovalcik et al. "Properties of scaffolds prepared by fused deposition modeling of poly(hydroxyalkanoates)". In: *Int J Biol Macromol* (2020).

[29] G. v Salmoria et al. "Mechanical properties of PA6/PA12 blend specimens prepared by selective laser sintering". In: *Polym Test* 31 (2012). DOI: 10.1016/j.polymertesting.2011.12.006.

[30] S.D. Nath and S. Nilufar. "An Overview of Additive Manufacturing of Polymers and Associated Composites". In: *Polymers* 12 (2020). DOI: 10.3390/polym12112719.

[31] A.D. Valino et al. "Advances in 3D printing of thermoplastic polymer composites and nanocomposites". In: *Prog Polym Sci* 98 (2019). DOI: 10.1016/j.progpolymsci.2019.101162.

[32] X. Ma D. Li J. Zhou and J. Li. "Synthesis of a novel biocomposite of poly (3-hydroxybutyrate-co-3-hydroxyhexanoate) reinforced with acetylated cellulose nanocrystals". In: *Cellulose* 26 (2019). DOI: 10.1007/s10570-019-02708-2.

[33] A.T. Sutton et al. "Powder characterisation techniques and effects of powder characteristics on part properties in powder-bed fusion processes". In: *Virtual Phys Prototyp* 12 (2017). DOI: 10.1080/17452759.2016.1250605.

Books

[12] Adrian P. Mouritz. *Introduction to Aerospace Materials*. Woodhead Publishing in Materials, 2012.

[25] J.D. Ferry. *Viscoelastic Properties of Polymers*. 3rd. New York: John Wiley & Sons, 1980.

Other references

Software used

[34] Blender Foundation. *Blender*. 2022. URL: https://www.blender.org.

[35] Prusa Research. *PrusaSlicer*. 2022. URL: https://www.prusa3d.com.

[36] Øyvind Kolås; Jehan Pagès and many others. *GNU Image Manipulation Program*. URL: https://www.gimp.org/.

[37] The Inkscape Project. *Inkscape*. URL: https://inkscape.org/.

[38] Pixelmator Team. *Pixelmator Pro*. 2022. URL: https://www.pixelmator.com/pro/.

[39] KDE. *Labplot*. 2022. URL: https://labplot.kde.org.

[40] John W. Eaton and many others. *GNU Octave*. 2020. URL: https://www.gnu.org/software/octave/index.

[42] Linus Torvalds. *git*. 2020. URL: https://git-scm.com/.

[43] Leslie Lamport. *LaTeX*. 2022. URL: https://www.latex-project.org/.